



Prevention of microgliosis halts early memory loss in a mouse model of Alzheimer's disease

Mandy S.J. Kater^{a,1}, Christiaan F.M. Huffels^{b,1}, Takuya Oshima^c, Niek S. Renckens^b, Jinte Middeldorp^{b,d}, Erik W.G.M. Boddeke^{c,e}, August B. Smit^a, Bart J.L. Eggen^c, Elly M. Hol^{b,2}, Mark H.G. Verheijen^{a,2,*}

^a Department of Molecular and Cellular Neurobiology, Center for Neurogenomics and Cognitive Research, Amsterdam Neuroscience, Vrije Universiteit Amsterdam, Amsterdam, The Netherlands

^b Department of Translational Neuroscience, University Medical Center Utrecht Brain Center, Utrecht University, Utrecht, The Netherlands

^c Department of Biomedical Sciences of Cells & Systems, Section Molecular Neurobiology, University Medical Center Groningen, University of Groningen, Groningen, The Netherlands

^d Department of Neurobiology & Aging, Biomedical Primate Research Centre, Rijswijk, The Netherlands

^e Center for Healthy Ageing, Department of Cellular and Molecular Medicine, University of Copenhagen, Copenhagen, Denmark

ARTICLE INFO

Keywords:
Alzheimer
Minocycline
Microglia
APP/PS1
Microgliosis

ABSTRACT

Alzheimer's disease (AD) is a neurodegenerative disorder characterized by cognitive decline, the neuropathological formation of amyloid-beta (A β) plaques and neurofibrillary tangles. The best cellular correlates of the early cognitive deficits in AD patients are synapse loss and gliosis. In particular, it is unclear whether the activation of microglia (microgliosis) has a neuroprotective or pathological role early in AD. Here we report that microgliosis is an early mediator of synaptic dysfunction and cognitive impairment in APP/PS1 mice, a mouse model of increased amyloidosis. We found that the appearance of microgliosis, synaptic dysfunction and behavioral impairment coincided with increased soluble A β ₄₂ levels, and occurred well before the presence of A β plaques. Inhibition of microglial activity by treatment with minocycline (MC) reduced gliosis, synaptic deficits and cognitive impairments at early pathological stages and was most effective when provided preventive, i.e., before the onset of microgliosis. Interestingly, soluble A β levels or A β plaques deposition were not affected by preventive MC treatment at an early pathological stage (4 months) whereas these were reduced upon treatment at a later stage (6 months). In conclusion, this study demonstrates the importance of early-stage prevention of microgliosis on the development of cognitive impairment in APP/PS1 mice, which might be clinically relevant in preventing memory loss and delaying AD pathogenesis.

1. Introduction

Human aging often comes with mild cognitive impairment that may progress into dementia, of which Alzheimer's disease (AD) is the most common form worldwide. The main pathological hallmarks of this neurodegenerative disorder are the deposition of extracellular amyloid-beta (A β) plaques and the hyper-phosphorylation of intracellular tau leading to tangle formation (Sasaguri et al., 2017). However, the severity of cognitive impairment does not correlate well with A β deposition (Ganz et al., 2018; Perez-Nievas et al., 2013; Westerman et al.,

2002) while there is a strict correlation with the loss of hippocampal synapses and glial reactivity (gliosis) (Merluzzi et al., 2018; Scheff et al., 2006). The majority of human risk genes for AD are highly, and several selectively, expressed by microglia (Wightman et al., 2021), thereby implicating microglia involvement in dementia. Therefore, the role of glia-related mechanisms has recently gained more interest as an element in AD pathology.

Microglia are the main tissue-resident macrophages of the brain and are important players in AD. There is abundant evidence for the reactivity of microglia (microgliosis) in the pathogenesis of AD (De Strooper

* Corresponding author.

E-mail address: mark.verheijen@vu.nl (M.H.G. Verheijen).

¹ Shared first.

² Shared last.

& Karran, 2016). The most characteristic feature of microgliosis is the change in cellular morphology, observed as a transition from ramified into a more amoeboid shape (Gomez-Nicola & Perry, 2015). In addition, in people with AD and in AD mice there is a clear change in microglia transcriptome, showing immune activation (Gerrits et al., 2021; Holtman et al., 2015; Kamphuis et al., 2016; Kamphuis et al., 2012; Orre et al., 2014). Reactive microglia release cytokines causing damage to healthy brain structures (Querfurth & LaFerla, 2010). Via complement-dependent pathways, reactive microglia show increased pruning of synapses leading to excessive synapse loss early in AD and ultimately cognitive impairment (Bessis et al., 2007; Hammond et al., 2018; Kettenmann et al., 2013; Paolicelli et al., 2011; Schafer et al., 2012).

Several recent studies on AD aimed to inhibit microgliosis, and associated AD pathology, using the tetracycline derivative minocycline (Biscaro et al., 2012; Howard et al., 2020; Mattei et al., 2017; Parachikova et al., 2010; Seabrook et al., 2006). Minocycline decreases the inflammatory activation of microglia (Mattei et al., 2017), and was shown to inhibit microgliosis and alleviate defects in synaptic plasticity and cognitive behavior in mouse models of AD (Biscaro et al., 2012; Mattei et al., 2017; Parachikova et al., 2010; Seabrook et al., 2006). Although these studies applied minocycline treatment at a relative early pathological phase, gliosis and A β plaques were already apparent. The efficacy of a preventive treatment with minocycline, before the onset of gliosis and amyloid pathology has not yet been determined. This is particularly relevant because a recent clinical study on patients with mild AD, showed that minocycline treatment was not successful in slowing disease progression (Howard et al., 2020). This implies that a too late treatment is not successful, but leaves the possibility that inhibition of microgliosis can be effective when targeted at an early AD stage, before microgliosis becomes apparent.

The APPswe/PS1dE9 (APP/PS1) mouse is a transgenic model for increased amyloidosis, resulting from the introduction of human disease-related mutations, one in amyloid precursor protein (APP) and one in presenilin 1 (PSEN1) (Jankowsky et al., 2004). Whereas these transgenic mouse models do not reproduce the full spectrum of pathological and clinical symptoms observed in AD, they are useful in studying early pre-pathological memory and plasticity impairments due to increased amyloidosis (Hijazi et al., 2019; Marchetti & Marie, 2011; Véghe et al., 2014). Previous studies on the early pathology in APP/PS1 mice revealed accumulation of A β monomers and oligomers, in both cortex and hippocampus, in the absence of A β plaque deposits (Van Tijn et al., 2012). Interestingly, alterations of long-term potentiation (LTP) and cognitive deficits were already observed before the presence of hippocampal A β plaques (Hijazi et al., 2019; Véghe et al., 2014). Here, we determined the temporal onset of microgliosis, in relation to other AD pathological parameters, in APP/PS1 mice. Subsequently, the outcome of preventive inhibition of microgliosis on AD-related disease progression was investigated. Our data establish that microglial reactivity is driving early-phase AD pathology and that early treatment is effective in preventing the resulting cognitive impairments.

2. Material and methods

2.1. Animals

APP/PS1 mice (The Jackson Laboratory; strain B6;C3-Tg(APPswe, PSEN1dE9)85Dbo/J; stock number 004462) express a chimeric mouse/human APP gene harboring the Swedish double mutation K595N/M596L (APPswe) and a human PS1 gene harboring the exon 9 deletion (PS1dE9), both under the control of the mouse prion protein promoter (MoPrP.Xho) (Jankowsky et al., 2004). APP/PS1 and wild type (WT) littermates were bred in-house, at both the Vrije Universiteit Amsterdam and Utrecht University, and maintained on a C57BL/6 background. Only male mice were included in the experiments unless specified otherwise. Mice were group-housed, except for behavioral assays. All cages were enriched with sawdust bedding, nesting material

and a gnawing stick. Housing was controlled for temperature ($\sim 21^\circ\text{C}$), humidity ($\sim 50\text{--}55\%$) and 12 h light–dark cycle. All experimental procedures were approved by the local animal research committees and comply with the European Council Directive 2010/63/EU.

2.2. Behavioral tests

All behavioral experiments were performed with male mice in the morning of the light phase. Mice were handled for two consecutive days prior to behavioral testing to reduce stress induced by the experimenter. All behavioral experiments were performed in sequence on the same group of animals, as described in the figures.

2.2.1. Morris water maze

Spatial memory was tested in a Morris water maze (MWM) task as previously described (Hijazi et al., 2019). In short: A pool was filled with water and contained a submerged escape platform. Visual cues were located at every quadrant at a distance of ~ 1 m. The training period lasted for four consecutive days using four trials/day. In each trial, the mice were placed into the water bath at a randomized start position and swam until the platform was reached. On day five, the probe test was performed in which the platform was removed from the water bath. Mice were placed in the water on the opposite side of where the platform was originally located and allowed to swim for 60 s. The parameter measured during the training trials was the mean latency (measured over 4 trials/day) to find the platform. During the probe test, the time spent in each quadrant of the pool was measured as well as swimming velocity. Spatial memory was assessed as the amount of time spent in the target quadrant.

2.2.2. Fear conditioning

Contextual fear conditioning was performed in a room with dimmed lights and continuous background noise (65 dB). Two mice were tested simultaneously in individual transparent acrylic chambers (25 cm \times 18 cm \times 21 cm; San Diego Instruments) with a floor of stainless-steel rods connected to a shock generator. Video images were recorded at a frame rate of 30 frames per second. A 2 min baseline recording was performed before providing the first foot-shock (0.7 mA, 2 s), followed by two more foot-shocks with a 30 s interval. The retrieval test was performed 48 h later in which the mice were placed in the fear conditioning box for ~ 210 s without foot-shocks. Freezing behavior was recorded when a mouse was not moving for a minimum of 30 frames. Accordingly, the percentage of freezing during the retrieval session was computed. The cages were cleaned with 70 % ethanol between each individual trial.

2.2.3. Nesting test

Mice were housed overnight in a novel cage containing sawdust bedding and a pressed cotton square (5 cm \times 5 cm). The test started in the afternoon 3 h before the start of the dark phase and ended 1 h after the lights were on the next morning. The quality of the nests was assessed by three individual blinded observers. The nests were scored according to a five-point scale as described earlier (Deacon, 2006). Scores were given as (1) cotton nestlet $> 90\%$ intact; (2) cotton nestlet 50–90 % intact; (3) cotton nestlet $< 50\%$ intact, material shredded over the cage with no identifiable nest; (4) flat identifiable nest; (5) identifiable nest within a quarter of the cage with walls higher than the mouse body size (Fig. S1a). Scores were averaged per experimental group.

2.2.4. Open field

Anxiety-like behavior and locomotor activity was assessed during the open field task as described before (Cetereisi et al., 2019). In short, mice naïve to the open field box were placed in the arena and allowed to explore for 10 min. Enhanced anxiety-like behavior was determined when mice spent less time in the inner zone. In addition, velocity was measured as parameter of locomotor activity. In between sessions, the sawdust bedding was shuffled to remove scent tracks of previous mice

and the walls of the arena were cleaned with 70 % ethanol.

2.3. Minocycline treatment

The mice received a daily oral dose of 50 mg/kg minocycline dissolved in 50 μ l of dehydrated unsalted dairy butter (method adapted from Aarts et al., 2015). The decision for oral treatment was made after a pilot experiment with 50 mg/kg minocycline dissolved in PBS provided per intra peritoneal injection that caused weight loss (>8%), peritoneal inflammation and several cases of death (data not shown). This was only observed in minocycline-treated mice (both WT and APP/PS1) and not in the vehicle-treated groups. Minocycline is well absorbed in the gastrointestinal tract (Blum et al., 2004) and will cross the blood–brain barrier (Yong et al., 2004) and therefore the oral route of administration is suitable. The dehydrated butter was warmed until melted and consequently used to dissolve minocycline into a stock concentration of 25 mg/ml. To administer minocycline in a concentration of 50 mg/kg mouse body weight, mice were weighted once a week and the calculated volume was pipetted onto a small petri dish (ϕ 35 mm) and cooled in the fridge until solidified again. Mice received a petri dish with minocycline droplet in the cage and were allowed for voluntary intake. The petri dishes were removed from the cage after the complete droplet was consumed. For vehicle treatment, a droplet containing solely dehydrated butter was used.

2.4. Electrophysiology

2.4.1. Field excitatory postsynaptic potentials (f-EPSP)

Acute coronal slices of the hippocampus were obtained from male and female APP/PS1 mice and littermate controls. Following decapitation, the brains were rapidly removed and stored in ice-cold oxygenated slicing artificial cerebrospinal fluid (aCSF; 300 mOsm, pH adjusted 7.35, in mM: 139 Choline Cl, 3.5 KCl, 1.25 NaH_2PO_4 , 0.5 CaCl_2 , 6 MgSO_4 , 10 Glucose, 25 NaHCO_3). Hippocampal slices (350 μ m) were then prepared on a Leica VT1000S vibratome using ice-cold slicing aCSF. Slices were incubated at room temperature (RT) in recording aCSF (300 mOsm, pH adjusted 7.35, in mM: 120 NaCl, 3.5 KCl, 1.25 NaH_2PO_4 , 2.5 CaCl_2 , 1.3 MgSO_4 , 10 Glucose, 25 NaHCO_3) for at least 1 h. f-EPSP recordings were performed in recording aCSF at $32 \pm 1^\circ\text{C}$. Stimuli were delivered in the stratum radiatum of the CA1 with a concentric bipolar tungsten stimulus electrode at 0.033 Hz (World Precision Instruments, Berlin, Germany). The half-maximum stimulus intensity was determined by obtaining an input–output curve and then fixed for every slice individually. LTP was induced by 1 train of 100 stimuli at 100 Hz (D'Amelio et al., 2011). f-EPSP signals were amplified and low-pass filtered at 2 kHz using an Axopatch 200B amplifier (Axon).

2.4.2. Whole-cell patch-clamp recordings

Hippocampal brain slices were prepared from male and female mice on a Leica VT1000S vibratome using slicing aCSF (300 mOsm, pH adjusted 7.35, in mM: 92 Choline Cl, 2.5 KCl, 1.2 NaH_2PO_4 , 25 NaHCO_3 , 0.5 CaCl_2 , 7 MgSO_4 , 20 2-[4-(2-hydroxyethyl)piperazin-1-yl]ethanesulfonic acid (HEPES), 25 Glucose, 20 N-methyl-D-glucamine (NMDG), 10 Sodium Ascorbate, 2 Thiourea, 3 Sodium Pyruvate, 3.1 N-acetyl-L-cysteine). Slices were then incubated in slicing aCSF for 10 min at 36°C and subsequently stored in incubation aCSF (300 mOsm, pH adjusted 7.35, in mM: 92 NaCl, 2.5 KCl, 1.2 NaH_2PO_4 , 30 NaHCO_3 , 2 CaCl_2 , 2 MgSO_4 , 20 HEPES, 25 Glucose, 3 Sodium Ascorbate, 2 Thiourea and 3 Sodium Pyruvate) for at least 1 h or until further use. Miniature excitatory postsynaptic currents (mEPSCs) were recorded as described in (Huffels et al., 2022). In short, CA1 pyramidal neurons were whole-cell patch-clamped in recording aCSF (300 mOsm, pH adjusted 7.35, in mM: 124 NaCl, 2.5 KCl, 1 NaH_2PO_4 , 26 NaHCO_3 , 2.5 CaCl_2 , 1.3 MgSO_4 , 5 HEPES, and 11 Glucose) at 32°C in the presence of 1 μM tetrodotoxin. For spine density quantification in vehicle- and minocycline-treated conditions, patch pipettes additionally contained 0.5 % biocytin to

allow for morphological reconstruction and spine density quantification. All cells were patched using borosilicate glass patch pipettes (Science Products) with resistance of 3–4 M Ω (300 mOsm, pH adjusted 7.3, in mM: 139 CsMSF, 5 CsCl, 2 MgCl_2 , 0.2 EGTA, 10 HEPES, 10 Creatine Phosphate, 4 $\text{Na}_2\text{-ATP}$, and $\text{Na}_3\text{-GTP}$). Recordings were amplified and low-pass filtered at 5 kHz using an Axopatch 200B amplifier (Axon). Data were excluded when the series resistance changed >15 %. All solutions mentioned above were continuously perfused with 95 % O_2 and 5 % CO_2 .

2.5. Immunohistochemistry and analysis of gliosis, A β plaques and neuronal spines

2.5.1. Immunohistochemistry

Mice were transcardially perfused with 4 % paraformaldehyde (PFA) in 0.1 M phosphate-buffered saline (PBS) after sedation with Avertin (250 mg/kg). Brains were dissected and kept in 4 % PFA for 24 h at 4°C followed by 30 % sucrose in PBS for cryoprotection, and stored at -80°C until further processing. The brains were sliced on a cryostat into 20 μm -thick coronal sections including the hippocampus and were stored free-floating in PBS with 0.02 % sodium azide. For morphometrics analysis of microglia morphology, heat-induced epitope retrieval was performed by placing the sections in sodium citrate (pH = 6.0) followed by microwave heating for 10 min. Next, blocking endogenous peroxidase activity was performed using 0.3 % hydrogen peroxide for 30 min at RT. To prevent nonspecific antibody binding, the sections were incubated in blocking solution (0.2 % Triton-X (Sigma Aldrich), 2.5 % bovine serum albumin (Sigma Aldrich) and 5 % normal goat serum (Sigma Aldrich) in PBS for 1 h at RT. Sections for morphometrics analysis were blocked with 5 % normal donkey serum only. Subsequent incubation with the primary antibody in blocking solution occurred at 4°C over night (o/n). The following primary antibodies were used: mouse-anti-IBA1 (1:1000, Abcam, Ab178847), rabbit-anti-CD68 (1:100, Novus Biologicals, NB100-683) and mouse-anti-6E10 (1:1000, ITK Diagnostics, SIG-39320) and for morphometrics analysis rabbit-anti-IBA1 (1:1000, WAKO, 019-19741 in 0.1 % Triton-X and 1 % normal donkey serum). Next, slices were incubated with secondary antibody in blocking solution at RT for 1 h: goat-anti-rabbit Alexa 568 (1:400, Fisher Emergo, A11011) or goat-anti-mouse Alexa 488 (1:400, Fisher Emergo, A11001). For morphometrics analysis biotinylated donkey-anti-rabbit (1:400, Jackson ImmunoResearch, 711-065-152) was used followed by incubation in ABC solution at RT for 30 min (VECTASTAIN[®] ABC Kit, Vector Laboratories, PK-6100) and finally visualization of IBA1-immunoreactivity by 3,3'-diaminobenzidine (DAB). To stain biocytin-filled neurons, hippocampal slices were incubated with a secondary antibody solution (2 % normal donkey serum, 0.13 % Triton-X in PBS) containing a streptavidin-Alexa594 conjugated antibody (Invitrogen, S11227, 1:1000) for 48 h. Slices were washed with PBS for 30 min and mounted on microscopy slides. Sections for the analysis of gliosis parameters and A β were stained with DAPI (1:250, Thermo-Fisher, D3571) at RT for 10 min and mounted on glass slides using polyvinyl alcohol anti-fading mounting medium with DABCO[™] (Sigma-Aldrich). A Golgi-Cox staining was performed on brain tissue collected after decapitation and rapid dissection of the brain. The staining was performed according to the FD Rapid GolgiStain[™] Kit (FD NeuroTechnologies Inc., PK401).

2.5.2. Imaging and analysis of gliosis

Immunofluorescent images were acquired using a Nikon A1 confocal microscope with NIC-Elements acquisition software. Three z-stack images (stack size 1 μm) were taken of the hippocampal CA1 region of each brain slice. Image rendering and analysis were performed in ImageJ. The number of IBA1⁺ cells was counted using the “cell counter” plugin. For CD68/IBA1 analysis the outlines of each IBA1⁺ cell were traced based on the IBA1 signal, and compared to the CD68 signal. Intensity was measured as the “mean grey value” parameter in ImageJ: the sum of the measured pixels divided by the number of pixels. For A β plaques

analysis, we first determined the outlines of cortex and hippocampus, and the plaque density was subsequently determined by a brightness-dependent threshold analysis of the A β signal per brain region. All analyses were performed by an experimenter blinded for the experimental conditions.

Scanning of brain sections for morphometrics analysis was done on a NanoZoomer 2.0-HT scanner (Hamamatsu Photonics, Japan). Single-cell images of microglia in the CA (CA1, CA2, CA3) were selected and processed for morphometric analysis as described previously (Zhang et al., 2021). A list of the morphometric parameters with explanations are provided in Supplemental Table S1. In total, 234 single images of microglia ($n > 17$ per animal, with $n = 3$ animals per group) were selected for analysis. A hierarchical clustering on principal components approach was used to identify and compare microglia subpopulations between experimental groups.

2.5.3. Spine density analysis

Pyramidal neurons in the hippocampal CA1, of both male and female mice, were imaged and digitized on a Zeiss automated bright-field M2-microscope (Zeiss, Germany) at 630x magnification using a 500 nm z-axis step size. The analyzed pyramidal cells were evenly distributed over the hippocampal CA1 area. Cells were included in the analysis when i) consistently stained over the full extent of the apical and basal dendritic trees and ii) their location was relatively isolated from neighboring cells. At least four CA1 pyramidal neurons per animal per condition were used for analysis. Analysis of apical and basal secondary dendrites was performed according to (D'Amelio et al., 2011). Quantification of individual spine types was performed based on classifications mentioned previously (Risher et al., 2014). All imaging, tracing, and analyses were performed by a researcher blinded for experimental conditions. Biocytin-filled cells were imaged by collecting confocal z-stack (500 nm z-axis step size) images using an Olympus confocal FV1000 microscope at 630x magnification and 1024x1024 resolution. The ImageJ plugin "TransformJ" was used to increase the functional resolution (Meijering et al., 2001). The spine density at secondary branches of the apical dendritic tree was then quantified automatically with Imaris (Oxford Instruments) software using the built-in filament tracer module using a similar inclusion strategy as described above.

2.6. ELISA

The human amyloid-beta 42 ELISA kit (Invitrogen, CA, USA) was used to quantify the levels of soluble human A β_{1-42} (A β_{42}) in mouse hippocampus homogenate. Sample preparation was performed according to the manufacturer's protocol. In short, duplicates of diluted hippocampus homogenate samples, standard curve samples and controls were loaded onto a 96-wells plate, mixed with A β_{42} detection antibody solution and incubated for 3 h. The samples were subsequently exposed to anti-rabbit HRP, stabilized chromogen and stop solution, with washing steps in between. Absorbance was determined for each well at 450 nm using a microplate reader (Thermo Fisher). For data representation, the values were normalized to total protein input as determined by Bradford assay (BioRad). Values were averaged per group and mean WT (non-transgenic) values were subtracted as background to obtain the final human A β_{42} levels.

2.7. Immunoblotting

Mouse hippocampus homogenate was used to analyse the expression levels of APP protein in mice that were treated with or without minocycline up to the age of 6 months. The total protein concentration in each sample was determined by Bradford assay (BioRad). Samples were diluted in SDS sample buffer and denatured at 95 °C for 5 min. The proteins were separated on a 4–15 % gradient SDS-PAGE gel (Criterion TGX Stain-Free Gel, BioRad) and electroblotted onto a methanol activated polyvinylidene membrane (PVDF, BioRad). Membranes were

incubated o/n at 4 °C with a mouse-anti-APP primary antibody (1:2000, BioLegend, SIG-39320) followed by incubation with a secondary goat-anti-mouse HRP conjugated antibody (1:10000, Dako) for 2 h at RT. Immunodetection was performed using Chemiluminescence Femto detection (Super Signal West Femto Maximum Sensitivity Substrate, Thermo Scientific) and an Odyssey FC imaging system (Li-Cor). To correct for loading differences, the femto signal was normalized to the total protein amount from each sample detected by 2,2,2-Trichloroethanol (TCE) staining of the gel (Ladner et al., 2004). Quantification of the signal was performed using Image Lab (version 6.0.1, BioRad) and Image Studio Lite (version 5.2.5, Li-Cor).

2.8. Statistical analysis

Statistical analysis was performed using GraphPad Prism 9.0 software. Details on the statistical tests used, statistical values and n numbers for each (statistical) comparison can be found in supplemental table S2. In general: the data was tested for a normal distribution with the Kolmogorov-Smirnov test, for testing of the difference between two groups, either a two-tailed student's t -test was applied or the non-parametric Mann-Whitney U test when required. A nested test was applied for analyses where the data was embedded in several subgroups. A (nested) one-way analysis of variance (ANOVA) or Kruskal-Wallis test was used in case of more than two groups and a two-way ANOVA when there was more than one condition. Repeated measures ANOVA was used for data that was measured over time. Recommended post hoc tests were used. Graphs are representing mean \pm standard error of the mean (SEM). $P \leq 0.05$ was set for significance.

3. Results

3.1. Microgliosis appears in APP/PS1 mice at the age of 3 months, before A β plaque deposition

The first aim was to characterize the progression of early disease pathology in APP/PS1 mice. Therefore, APP/PS1 and WT littermates were studied at several timepoints between the age of 2 and 6 months (Fig. 1a), to determine immunohistological alterations in the hippocampal CA1. The number of microglia, stained for IBA1, was increased in APP/PS1 mice at the age of 3 months and further increased at 4 and 6 months of age (Fig. 1b, c). Expression of CD68 was used to detect microglia with potentially increased phagocytic activity, which was significantly increased at the age of 4 months onwards (Fig. 1b, d). Together, this shows the first appearance of microgliosis in the CA1 of the hippocampus of APP/PS1 mice at the age of 3 months, and a further increase at 4 and 6 months of age.

Next, a 6E10 antibody staining of amino acid residues 1–16 of human A β was used to determine the A β plaque load in APP/PS1 mice (Fig. 1e, f). This revealed that plaques were absent in cortex and hippocampus of APP/PS1 mice at the age of 3 months, and became increasingly apparent from 4 and 6 months on in both brain areas (Fig. 1g). In addition, frequency distribution analysis showed that 6E10⁺ plaque size in APP/PS1 mice appeared as small ($<100 \mu\text{m}^2$) at 4 months, in both cortex (Fig. 1h) and hippocampus (Fig. 1i), and increased to larger plaques (>101 – $200 \mu\text{m}^2$) at 6 months. Since smaller plaques are reflecting newly formed plaques, this suggests that most of these are formed starting at the age of 4 months. To quantify levels of soluble human A β_{42} , the major A β species in plaques, an ELISA assay was performed. We found that the level of soluble human A β_{42} in the hippocampus of APP/PS1 mice was elevated at 3 months and further increased at 6 months (Fig. 1j). Thus, the first appearance of microgliosis coincided with increased soluble A β_{42} levels, and occurred well before the presence of A β plaques.

3.2. Impairment of cognitive behavior in pre-plaque stage APP/PS1 mice

To further characterize early disease pathology in APP/PS1,

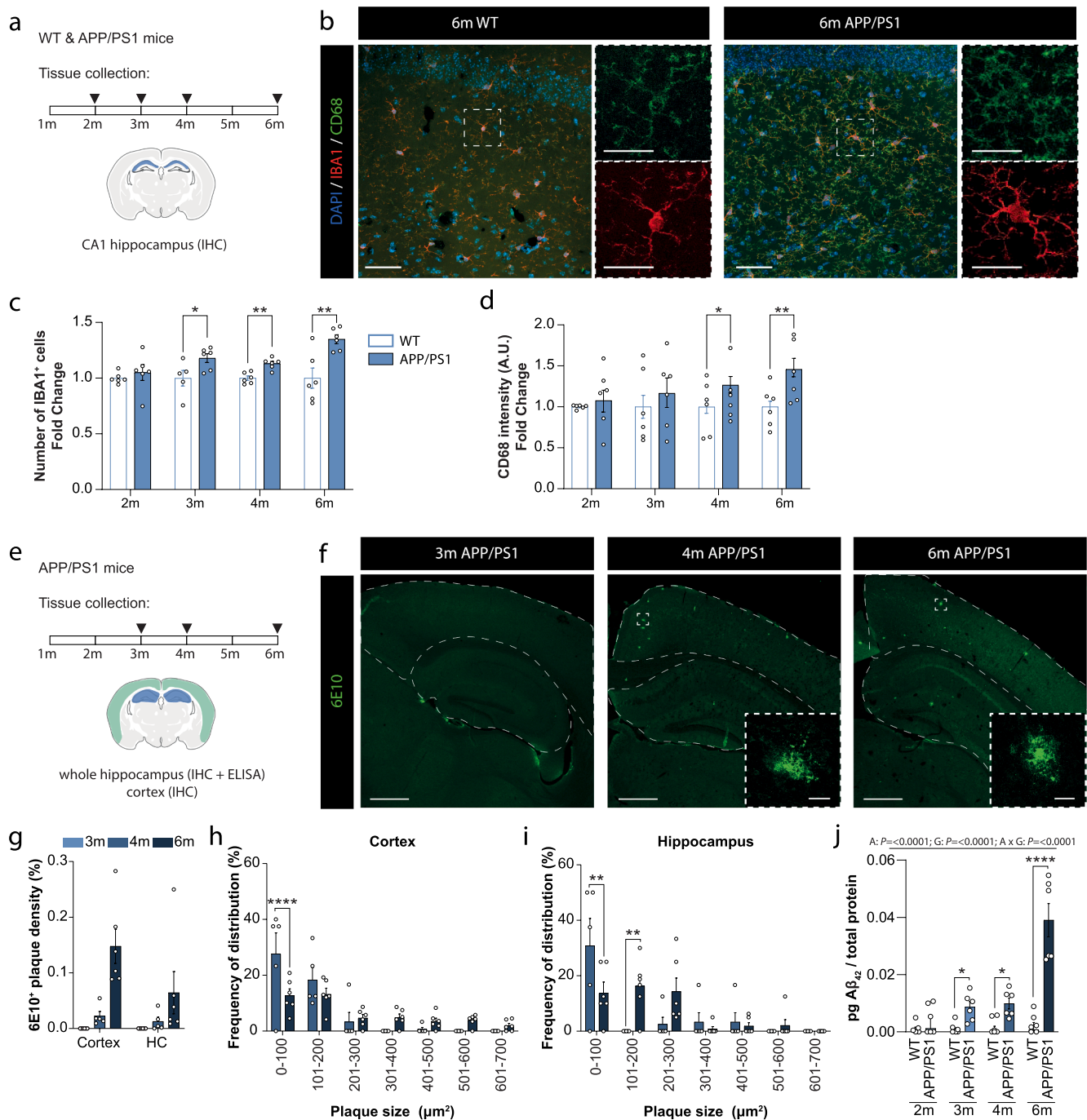


Fig. 1. Microgliosis appears in APP/PS1 mice at 3 months and before A β plaque deposition. **a)** Study design showing that tissue of WT and APP/PS1 mice was collected at the age of 2 months (m), 3 m, 4 m and 6 m. Immunohistochemistry (IHC) analysis was performed on the hippocampal CA1 stratum radiatum indicated in blue. **b)** Representative images of IBA1⁺ and CD68⁺ stained microglia in hippocampal CA1 of 6 months old WT (left) and APP/PS1 (right) mice. Scale bars in main images: 50 μ m, in insets: 20 μ m. **c)** Number of IBA1⁺ cells per field of view (225 \times 225 μ m). **d)** CD68 intensity in arbitrary units (A.U.) within the IBA1⁺ area. **e)** Study design showing that tissue of APP/PS1 mice was collected for analysis at the age of 3 m, 4 m and 6 m. IHC analysis was performed on whole hippocampus (in blue) and cortex (in green). ELISA analysis was performed on whole hippocampus. **f)** Representative images of 6E10⁺ plaques in cortex and hippocampus of 3 (left), 4 (middle) and 6 months old (right) APP/PS1 mice. Scale bars: main images: 500 μ m, insets: 25 μ m. **g)** Quantification of 6E10⁺ plaque density relative to total cortex or hippocampus area in 3-, 4- and 6-months old mice. **h, i)** Frequency distribution plot of plaque size (in bins of 100 μ m²) in cortex (**h**) and hippocampus (**i**). **j)** Levels of soluble human A β ₄₂ in whole hippocampus of 2-, 3-, 4-, and 6-months old WT and APP/PS1 mice. The detected A β ₄₂ levels were normalized to the total protein. Data in **c, d, e** is represented as fold change relative to WT levels per time point. Unpaired *t*-test (**fig. c, d**) or Two-way ANOVA (**fig. f-h**). *n* = 5–6 per group. See table S2 for full statistical details. **p* = <0.05; ***p* = <0.01; *****p* = <0.0001. All data is presented as mean \pm SEM.

potential cognitive deficits were assessed in separate batches of mice at 2, 3 or 4 months of age (**Fig. 2a**). The open-field experiment showed that anxiety-like behavior was not affected at any age (**Fig. S1b-d**), whereas locomotor activity was enhanced in APP/PS1 mice at 2 and 3 months

(**Fig. S1e-g**). Spatial memory was determined by MWM performance, which showed that APP/PS1 mice had a reduced latency to find the submerged platform during the training at 4 months (**Fig. 2b-d**), and a reduced preference for the target quadrant (TQ) in the probe trial at 3

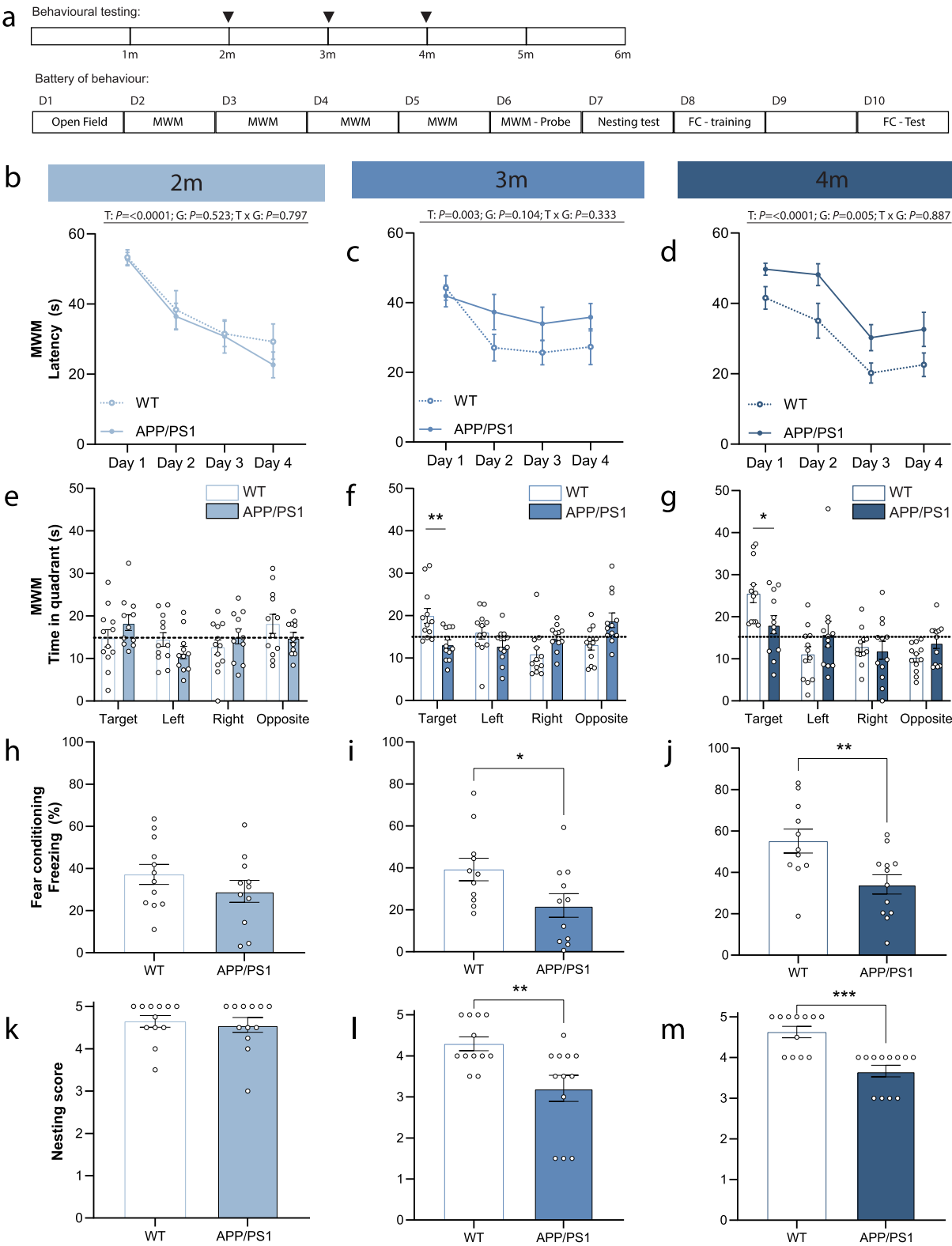


Fig. 2. Cognitive behavior is impaired in APP/PS1 mice from age 3 months onwards. **a**) Schematic overview of the workflow of behavioral experiments. The experimental assays were performed on consecutive days, lasting 10 days (D1-D10). **b-d**) Morris water maze (MWM) training latencies (seconds) to the platform measured over four training days in WT and APP/PS1 of 2 months (**b**), 3 months (**c**) and 4 months (**d**) of age. **e-g**) Time spent (seconds) in the MWM quadrants during the probe test, where the target quadrant is the quadrant with the original location of the platform. Measured in WT and APP/PS1 mice of 2 (**e**), 3 (**f**) and 4 months (**g**) of age. **h-j**) Freezing levels (%) measured during the contextual fear conditioning retrieval session 48 h after shock at 2 (**h**), 3 (**i**) and 4 months (**j**) of age. **k-m**) Nest building scores assessed during the nesting test in WT and APP/PS1 mice at 2 (**k**), 3 (**l**) and 4 months (**m**) of age. Repeated measures ANOVA (fig. **b-d**), Unpaired *t*-test (fig. **e, g-j**) or Mann-Whitney U (fig. **f, k-m**). *n* = 11–12 per group. See table S2 for full statistical details. * *p* = <0.05; ** *p* = <0.01; *** *p* = <0.001. Data are presented as mean ± SEM.

and 4 months (Fig. 2e–g). No differences in swimming velocity were observed (Fig. S1h–j). Together this indicates a spatial memory deficit in APP/PS1 mice from 3 months of age onwards. Next, contextual fear memory was tested by measuring freezing levels during a retrieval session, 48 h after a shock was given in a specific context. APP/PS1 mice showed reduced freezing levels at 3 and 4 months old (Fig. 2h–j), indicative for a contextual fear memory deficit starting at the age of 3 months. No clear differences were observed between genotypes during the acquisition phase of the fear conditioning task at any age (Fig. S1k–m). Finally, animals underwent a nest-building task, which is dependent on the hippocampus (Deacon et al., 2002), among other regions (Deacon, 2006) and similarly interpreted as dysexecutive task performance as clinically observed in AD patients (Filali et al., 2009; Neely et al., 2019). In this task, the quality of nest building was assessed (Fig. S1a), which revealed that APP/PS1 mice already showed impaired nest-building behavior at the age of 3 months (Fig. 2k–j). In conclusion, APP/PS1 mice show cognitive deficits from the age of 3 months onwards.

3.3. Hippocampal synaptic deficits in early-stage APP/PS1 mice

To determine whether the cognitive deficits of early-stage APP/PS1 mice coincide with neurophysiological alterations, the capability to induce synaptic plasticity was assessed in APP/PS1 and WT littermates at 2, 3 and 4 months. f-EPSPs were recorded from the hippocampal CA1 after extracellular stimulation of the Schaffer collaterals in hippocampal slices. LTP was induced by a high-frequency stimulus at half-maximum intensity (Fig. 3a). APP/PS1 mice and WT littermates were not

significantly different in the postsynaptic response before LTP induction. However, APP/PS1 mice showed significantly impaired levels of LTP at 4 months (Fig. 3b), while variable and not significantly different at 2 and 3 months (Fig. S2). As glutamatergic transmission is essential for the induction of postsynaptic plasticity, we next assessed the basic properties of glutamatergic transmission for WT and APP/PS1 mice (4 months) by recording mEPSCs of hippocampal CA1 pyramidal neurons and found that neither the frequency nor amplitude of excitatory glutamatergic events were significantly different (Fig. 3c, d).

Next, we assessed whether the impaired glutamatergic transmission in early-stage APP/PS1 mice is associated with reduced spine density, as has been demonstrated by several studies in both AD patients and AD mouse models (Hong et al., 2016; Jacobsen et al., 2006; Terry et al., 1991) including APP/PS1, however not for the pre-plaque stage (Shi et al., 2017). Using Golgi-Cox-stained brain slices, we quantified spines on apical and basal secondary dendrites of CA1 pyramidal neurons, and distinguished mature (i.e., mushroom) versus immature (i.e., thin, filopodia, stubby) spines (Fig. 3e). We found a significant decrease in the total number of spines at apical secondary dendrites of APP/PS1 mice at 4 months (Fig. 3f, g), which was primarily caused by a reduction in mature spines (Fig. 3h, i).

Together, these data show that synaptic plasticity is impaired in the hippocampal CA1 of early-stage APP/PS1 mice, which is associated with the loss of mature spines at specifically the apical secondary dendrites of CA1 pyramidal neurons.

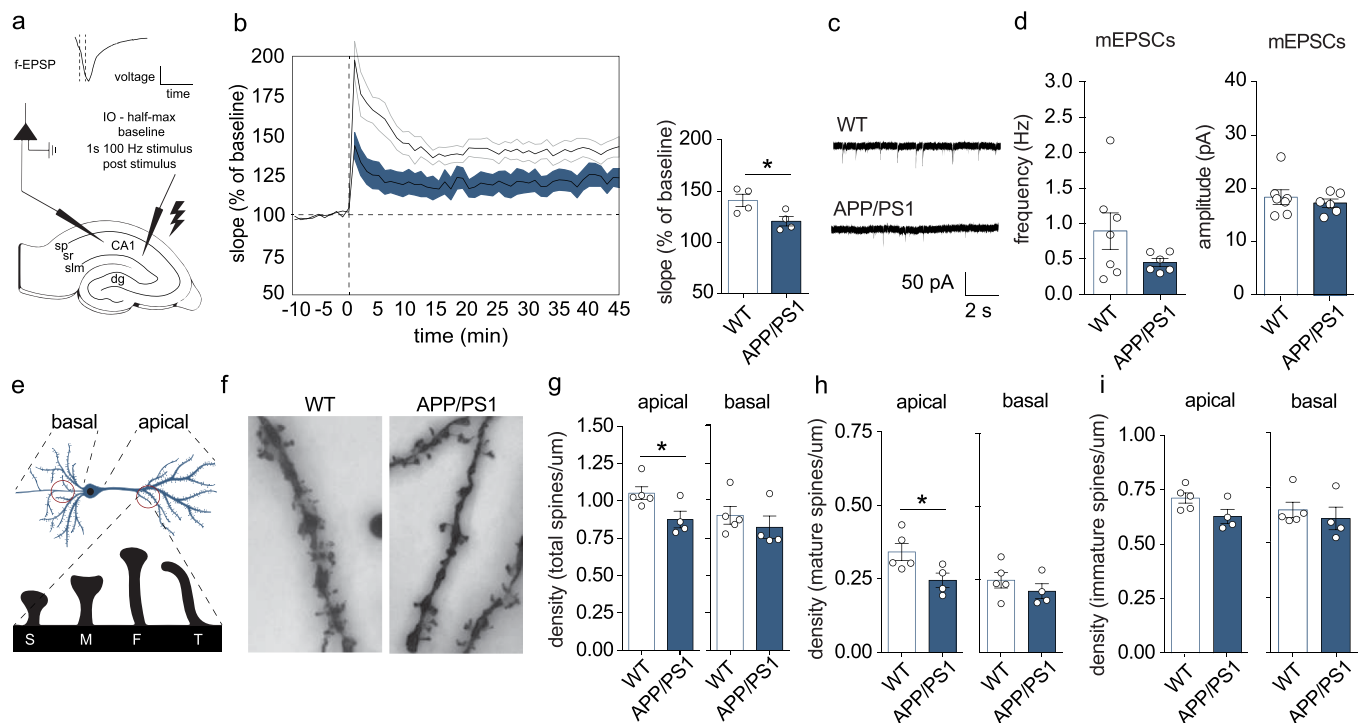


Fig. 3. Impaired LTP and loss of spines in early-stage APP/PS1 mice. a) Schematic overview. LTP was assessed in CA1 hippocampal slices of APP/PS1 mice and WT littermates by recording f-EPSPs. Brain regions: CA1, cornu ammonis area 1; SP, stratum pyramidale; SR, stratum radiatum; SLM, stratum lacunosum moleculare; DG, dentate gyrus. b) LTP traces for APP/PS1 and WT littermates. The middle and outer lines indicate the group average and SEM, respectively. The stimulus was administered at $t = 0$. The bar graphs show quantification of the post-tetanic data normalized to baseline. c) Representative mEPSC traces obtained from CA1 pyramidal neurons in APP/PS1 and WT littermates. d) Quantification of mEPSC frequency and amplitude. e) Schematic overview. Synaptic spines on apical and basal secondary dendritic branches of CA1 pyramidal neurons were quantified and compared between APP/PS1 and WT littermates. Spines were classified as stubby (S), mushroom (M), filopodia (F) or thin (T). f) Representative images showing a reduced total secondary dendritic spine density of CA1 pyramidal neurons in APP/PS1 mice. g) Quantification of apical and basal total secondary dendritic spine density of CA1 pyramidal neurons. h) Density of mature (mushroom) spines of secondary apical and basal dendrites. i) Density of immature (stubby, filopodia, thin) spines of secondary apical and basal dendrites. Unpaired t -test (b,e–i) or Mann-Whitney U (d). * $p < 0.05$. b: WT ($n = 8$, $N = 4$) vs APP/PS1 ($n = 8$, $N = 4$); d: (WT ($n = 15$, $N = 7$) vs APP/PS1 ($n = 18$, $N = 6$); e–i: WT ($n = 20$, $N = 5$) vs APP/PS1 ($n = 20$, $N = 4$). Data are presented as mean \pm SEM. See table S2 for full statistical details.

3.4. Minocycline effectively prevents microgliosis in early-stage APP/PS1 mice

With the implication of microglia in synaptic dysfunction and synapse loss in neuroinflammation and AD (Griffin et al., 2006; Hong et al., 2016; Rebola et al., 2011; Wang et al., 2005; Wang et al., 2015) we determined whether microgliosis, as observed above, may underlie the coinciding A β pathology, synaptic impairment and cognitive deficits in early-stage APP/PS1 mice. For this, mice received a daily voluntary oral treatment with 50 mg/kg minocycline, starting at 2 months (before microgliosis) until 4 months (when microgliosis, and synaptic and cognitive deficits are apparent) (Fig. 4a). Minocycline treatment did not negatively affect the general health of mice nor did it affect weight gain (Fig. S3). Immunohistochemical analysis at 4 months showed an increase in the number of IBA1⁺ cells in APP/PS1 vehicle-treated mice compared to WT vehicle-treated mice, which was completely prevented by treatment of APP/PS1 mice with minocycline (Fig. 4b, c).

Next, we performed a detailed morphometric analysis on CA1 microglia to determine changes in relation to the APP/PS1 genotype and minocycline treatment. Twenty three morphological parameters were determined in IBA1⁺ cells (Fig. 4d, Table S1). Then, cells were hierarchically clustered based on these parameters, resulting in 4 distinct clusters (Fig. 4e, f and Fig. S4). Sholl analysis revealed that microglia in each cluster show different sizes and ramifications, which is illustrated by the cell silhouettes of the most representative cell of each cluster (Fig. 4g, h). Microglia in cluster 1 are relatively large and highly ramified, indicative of surveilling or homeostatic microglia (Tremblay et al., 2011). Microglia in cluster 4 are relatively small and with high circularity, often associated with a more activated state (Leyh et al., 2021). Microglia in clusters 2 and 3 seem to be in intermediate states towards the activated state. Cluster 1 ‘homeostatic’ microglia were found in vehicle treated WT mice, and only in APP/PS1 mice when treated with minocycline (Fig. 4i). Remarkably, treatment of WT mice with minocycline also resulted in the absence of cluster 1 microglia. We next used the expression of CD68 to determine whether the shift in microglia morphology clusters was related to phagocytic activity, and found that CD68 levels were only upregulated in microglia of vehicle-treated APP/PS1 mice, while not in the minocycline-treated WT or APP/PS1 mice (Fig. 4j, k). Together, these results indicate that microglia display an increased reactive morphology in APP/PS1 mice, which is prevented by minocycline treatment. In addition, minocycline treatment also affected the morphology of microglia in WT mice, without affecting their phagocytic activity.

3.5. Prevention of microgliosis by minocycline rescues synaptic and cognitive deficits but not A β pathology in APP/PS1 mice of 4 months

The increased phagocytic activity of reactive microglia may play a role in the clearing of A β plaques and fibrils, as reported by a number of studies although with conflicting results (Biscaro et al., 2012; El-Shimy et al., 2015; Familian et al., 2006; Fan et al., 2007; Ferretti et al., 2012; Parachikova et al., 2010; Seabrook et al., 2006). We found that minocycline treatment from 2 months onwards seemed to reduce A β plaque density in APP/PS1 mice at 4 months ($p = 0.055$), most prominent in the cortex (Fig. 5a, b). No difference in plaque size was observed in the cortex (Fig. 5c) or the hippocampus (Fig. 5d). Furthermore, the hippocampus of 4 months old APP/PS1 mice contained strongly elevated levels of soluble A β_{42} , which were not affected by 2 months minocycline treatment (Fig. 5e). We conclude that the appearance of A β plaques or level of soluble A β_{42} in the hippocampus of early-stage APP/PS1 mice are not affected by 2 months long preventive minocycline treatment.

Next, we determined whether the cognitive impairment observed in APP/PS1 mice at 4 months (Fig. 2), was positively affected by the preventive 2 months treatment with minocycline (Fig. 6a). First, the open field task showed that minocycline treatment did not affect locomotor activity or anxiety-like behavior (Fig. S5a–b). The MWM task, to assess

spatial memory, showed that minocycline improved the reduced training performance of APP/PS1 mice at trend-level ($p = 0.066$) at day 3 (Fig. 6b), and fully and significantly rescued the reduced performance of APP/PS1 in the probe test (Fig. 6c). No differences in swimming velocity were observed (Fig. S5c). This indicates that minocycline treatment improved spatial memory in APP/PS1 mice. Minocycline also fully rescued the impaired contextual fear memory of APP/PS1 mice, as determined with the fear conditioning test (Fig. 6d). Minocycline did not affect the activity during the acquisition phase of this test (Fig. S5d). Finally, also the impaired nest building behavior of APP/PS1 mice was fully rescued by minocycline (Fig. 6e). We conclude that preventive minocycline treatment rescued the spatial memory, contextual fear memory and nesting behavior of 4 months old APP/PS1 without affecting these cognitive functions in WT mice.

We next assessed whether 2 months minocycline treatment also improved the impaired synaptic plasticity in the CA1 of 4 months APP/PS1 mice (as in Fig. 3). To that end, f-EPSPs were recorded in hippocampal brain slices of APP/PS1 and WT littermates (Fig. 7a) treated with either vehicle or minocycline. Postsynaptic baseline responses were similar between all groups. APP/PS1 mice showed reduced levels of LTP, which were fully rescued by minocycline treatment (Fig. 7b). Surprisingly, minocycline treatment significantly reduced LTP in WT mice (Fig. 7b).

As we previously found a reduced spine density in the CA1 of 4 months old APP/PS1 mice (Fig. 3), we now biocytin-filled CA1 pyramidal neurons to allow morphological reconstruction and determine the effect of minocycline on spine density (Fig. 7c). The total spine densities on secondary dendritic branches were in the same range as observed previously (Fig. 3g), and although spine density seemed to be reduced in APP/PS1 mice, this did not reach significance (Fig. 7d), making it not possible to draw any conclusions on the effect of minocycline treatment on spine density in the CA1 of 4 months old APP/PS1 mice.

Together, our data show that minocycline rescued the synaptic plasticity impairments in early-stage APP/PS1 mice, but also indicate that minocycline may affect CA1 synapse physiology under healthy conditions.

3.6. Efficacy of different minocycline treatments on gliosis, A β levels and cognitive behavior

To determine whether the treatment of AD pathology by minocycline is also persistently effective or when started after the onset of microgliosis, we tested 3 different treatment regimes: minocycline was given i) before microgliosis-continuously (2 till 6 months of age, MC 2–6 m), ii) before microgliosis-temporary (2 till 4 months, MC 2–4 m) or iii) after microgliosis (4 till 6 months of age, MC 4–6 m) (Fig. 8a). All 3 minocycline treatment regimes reduced the number of microglia in APP/PS1 mice, although treatment after the onset of microgliosis was less effective (Fig. 8b, d). Minocycline did not affect the number of microglia in WT mice. Similarly, none of the minocycline treatments affected microglial CD68 expression in WT mice, whereas all 3 regimes reduced CD68 expression in APP/PS1 mice, with treatment after the onset of microgliosis being less effective (Fig. 8c, d). Together, this indicates that minocycline treatment reduces microgliosis and phagocytic activity in APP/PS1 mice and is most effective when started before the onset of gliosis.

In line with our observation that preventive treatment with minocycline at 2–4 months did not significantly reduce A β plaque load in the cortex or hippocampus at 4 months (in Fig. 5), further aging of the animals until 6 months without treatment did not show an effect of earlier minocycline treatment on A β plaque load in cortex or hippocampus (MC 2–4 m; Fig. 8e, f). Also starting with minocycline after the onset of microgliosis (MC 4–6 m; Fig. 8e, f) did not significantly reduce A β plaque load. However, a preventive and continuous minocycline treatment (MC 2–6 m) was effective in reducing A β plaque density in the cortex, although not in the hippocampus. None of the treatment regimes

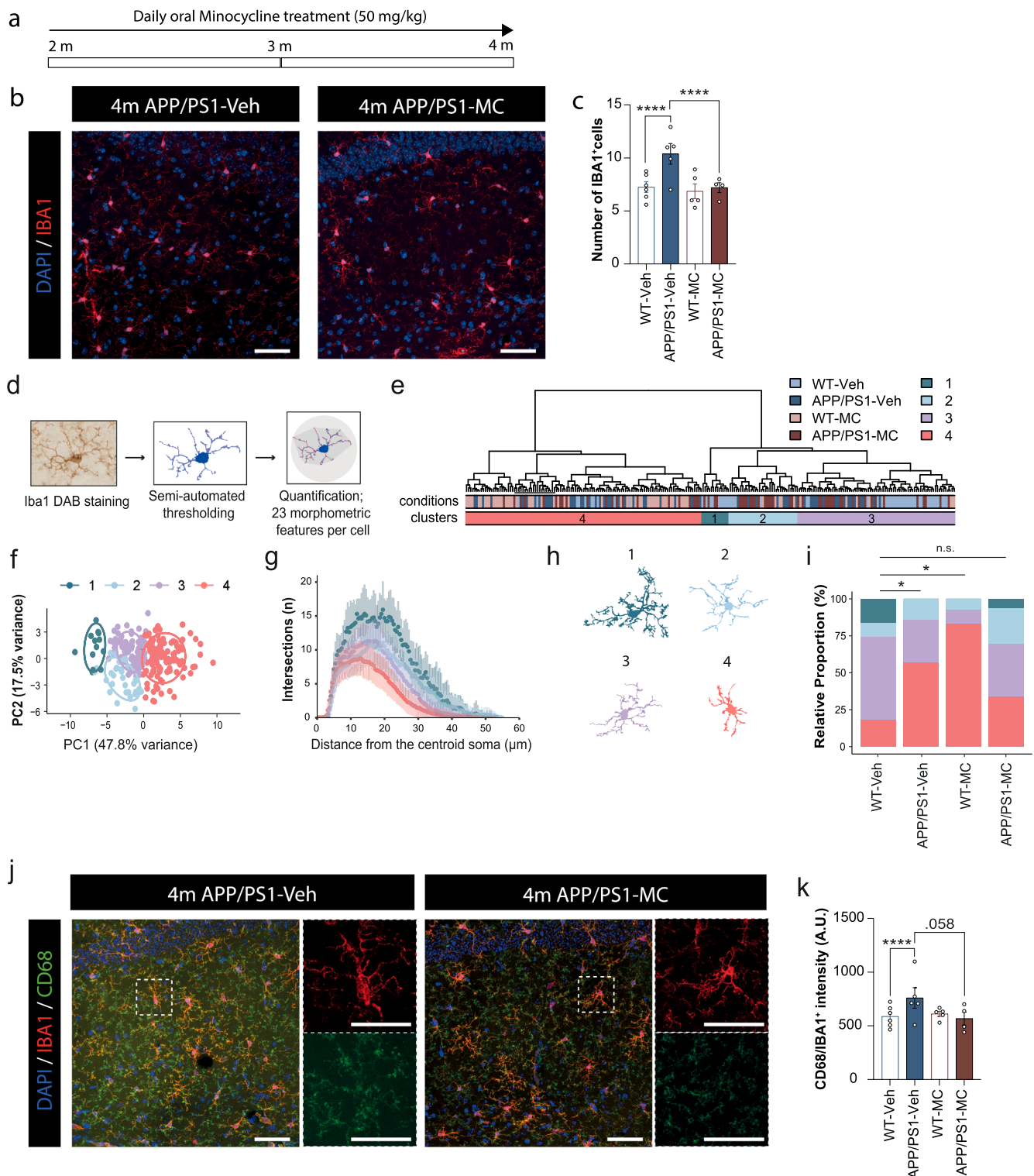


Fig. 4. Minocycline treatment prevents microgliosis in early-stage APP/PS1 mice. **a)** Schematic overview of the methods related to minocycline treatment. **b)** Representative images of IBA1⁺ stained microglia in hippocampal CA1 of APP/PS1 vehicle-treated mice (left) and APP/PS1 minocycline-treated mice (right). Scale bar: 50 μ m. **c)** Quantification of the number of IBA1⁺ cells measured per field of view (318.20 \times 318.20 μ m). **d)** Schematic overview of the morphometric analysis of microglia. **e)** Hierarchical clustering based on 23 morphological features (see Table S1 and Figure S4) with condition and cluster per cell. **f)** PCA plot shows all selected individual cells with corresponding colors of each cluster. The x and y axes represent the first and second principal components (PC1 and PC2), respectively. **g)** Sholl analysis of microglia from each cluster. **h)** Representative cell per cluster visualized as cell silhouettes. **i)** Bar plot showing frequency of cells per cluster in WT and APP/PS1 mice with vehicle and minocycline treatment with comparisons of cluster 1 proportions. **j)** Representative images of IBA1⁺ and CD68⁺ stained microglia. Scale bar in main images: 50 μ m. Scale bar in detailed images: 20 μ m. **k)** Quantification of CD68 staining intensity measured within IBA1⁺ area, in arbitrary units (A.U.). Nested one-way ANOVA (fig. c, k) or Kruskal-Wallis (fig. i). $n = 3-6$ per group. See table S2 for full statistical details. n.s. = non-significant; * $p < 0.05$; **** $p < 0.0001$. Data are presented as mean \pm SEM.

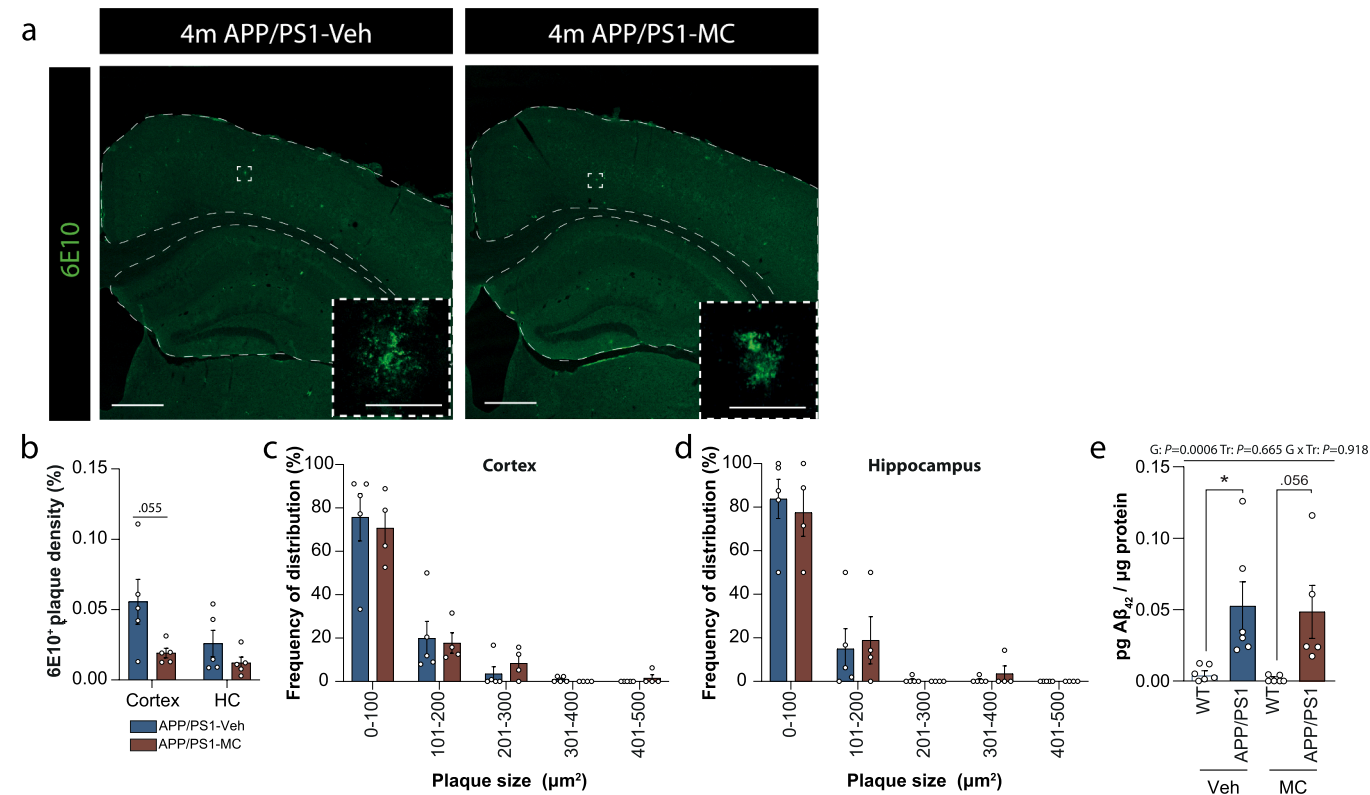


Fig. 5. Microgliosis-preventive minocycline treatment does not affect soluble nor aggregated Aβ levels in hippocampi of APP/PS1 mice at 4 months. a) Representative images of immunohistochemical staining for 6E10⁺ amyloid beta plaques. Scale bar main images: 500 μm. Scale bar zoom in: 25 μm. b) Quantification of 6E10⁺ plaque density relative to total cortex or hippocampus area. c) Frequency distribution plot of cortex data as presented in b. d) Frequency distribution plot of hippocampus data as presented in b. e) ELISA quantification of Aβ₄₂ levels measured per μg protein. Unpaired *t*-test (fig. b) or Two-way ANOVA (fig. c-e). *n* = 5–6 per group. See table S2 for full statistical details. * *p* = < 0.05. Data are presented as mean ± SEM.

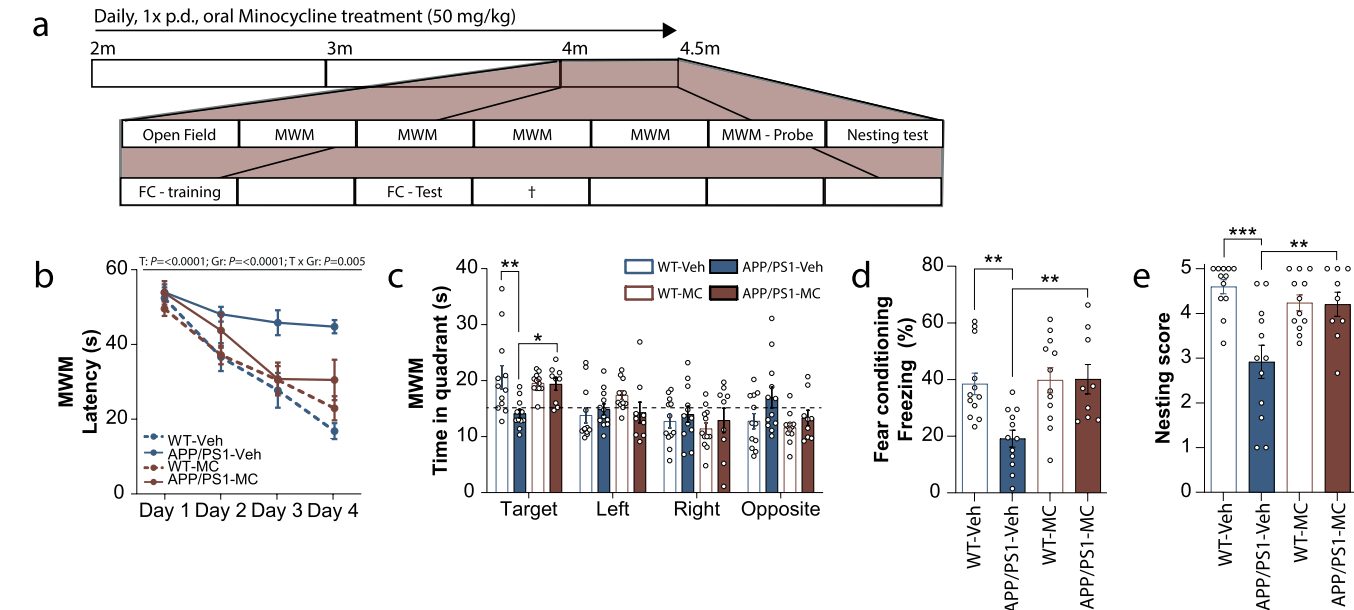


Fig. 6. Microgliosis-preventive minocycline treatment prevents cognitive deficits in 4 months old APP/PS1 mice. a) Schematic overview of the behavioral experiments. b) Morris water maze training latencies to platform (seconds) measured over four days. c) Morris water maze probe test performance, determined as the time spent (seconds) in each quadrant. The target quadrant is the quadrant with the original location of the platform. Dashed line indicates 25 % chance level of exploration. d) Freezing levels (%) measured during the retrieval session 48 h after shock. e) Nesting scores assessed during the nesting test. Repeated measures ANOVA (fig. b) or two-way ANOVA (fig. c-e). *n* = 9–12 per group. See table S2 for full statistical details. * *p* = < 0.05; ** *p* = < 0.01; *** *p* = < 0.001. Data are presented as mean ± SEM.

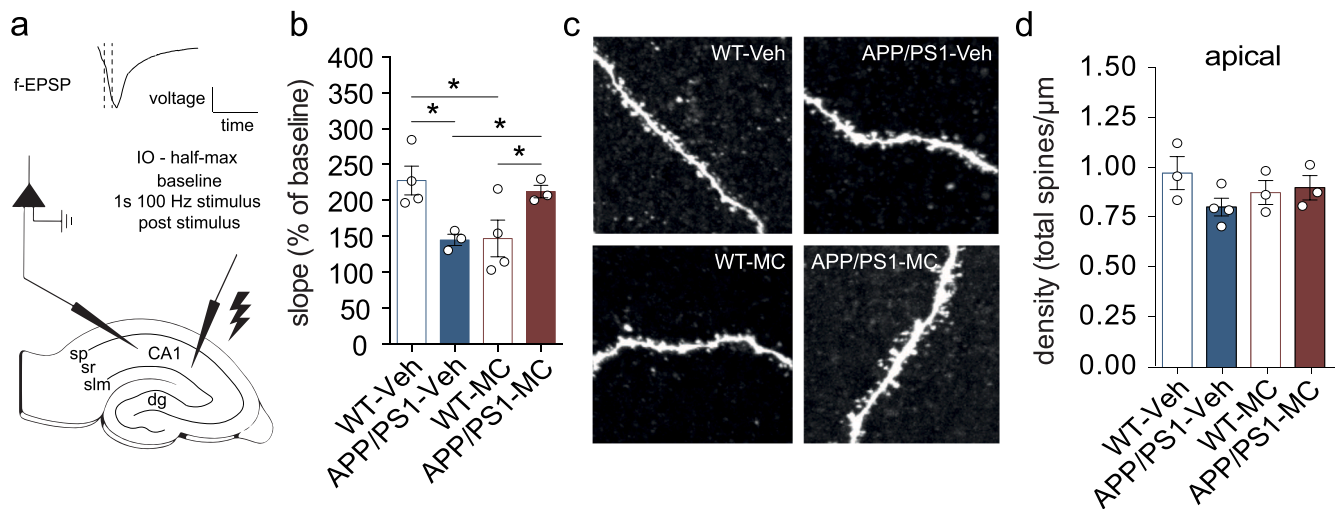


Fig. 7. Microgliosis-preventive minocycline treatment improves LTP in the CA1 of 4 months old APP/PS1 mice. **a)** Schematic experimental overview of the LTP experiment. f-EPSPs were recorded in CA1 hippocampal slices of vehicle- and minocycline-treated APP/PS1 and WT littermates. Brain regions: CA1, cornu ammonis area 1; SP, stratum pyramidale; SR, stratum radiatum; SLM, stratum lacunosum moleculare; DG, dentate gyrus. **b)** Quantification of changes in the f-EPSP slope relative to baseline for vehicle- and minocycline-treated WT and APP/PS1 mice. **c)** Representative images of biocytin-filled spines on apical secondary dendritic branches of CA1 pyramidal neurons of vehicle- and minocycline-treated APP/PS1 and WT mice. **d)** Quantification of apical total secondary dendritic spine density of CA1 pyramidal neurons in vehicle- and minocycline-treated APP/PS1 and WT mice. See table S2 for full statistical details (including n and N). * $p < 0.05$. Data are presented as mean \pm SEM.

influenced A β plaque size (Fig. 8g, h). Interestingly, while we showed that preventive treatment with minocycline at 2–4 months did not reduce soluble A β_{42} levels in the hippocampus of APP/PS1 mice at 4 months (Fig. 5), each of the three minocycline treatment regimes halved the levels of soluble A β_{42} levels in the hippocampus of APP/PS1 mice at 6 months of age (Fig. 8i), resulting in levels that were comparable to those of untreated APP/PS1 mice at 4 months of age (Fig. 1j, Fig. 5e). Consequently, we questioned whether minocycline may reduce A β level by altering APP protein expression. Immunoblotting revealed that APP expression was not affected by any of the minocycline treatments (Fig. S6).

To determine the effect of different minocycline regimes on cognitive function of APP/PS1 mice, we first assessed their performance in the nest building task at 2, 4 and 6 months of age (Fig. 9a). In line with earlier observations (Fig. 2k–m), nest building was normal for vehicle treated APP/PS1 mice at 2 months and impaired at 4 and 6 months of age (Fig. 9b). Similarly, as we showed in Fig. 6e, preventive minocycline treatment rescued nest building of 4 months old APP/PS1 mice for both the MC 2–4 m and MC 2–6 m groups (Fig. 9b). Importantly, continuous minocycline treatment until the age of 6 months sustained the improved nest building behavior of APP/PS1 mice, unlike APP/PS1 mice for which treatment had not continued from month 4–6 (MC2-4 m) and that showed impaired nest building at 6 months. Also, late minocycline treatment, after the onset of microgliosis did not improve nest building behavior of APP/PS1 mice (MC4-6). Next, the effect of the different treatment regimes on spatial memory of APP/PS1 mice at 6 months was determined. Whereas we showed in Fig. 6 that a preventive temporary minocycline treatment was sufficient to rescue spatial memory of APP/PS1 mice at 4 months, we observed that each of the minocycline treatment regimes were effective in improving spatial memory at 6 months, as observed for the partial rescued latencies of APP/PS1 mice to reach the platform during training (Fig. 9c), as well as for the fully rescued time spent in the TQ during the probe test (Fig. 9d). The minocycline treatment regimes did not affect the increased hyperactivity of APP/PS1 mice, as measured in the open field assay (Fig. S7b), nor on the swimming speed in the MWM (Fig. S7c) or the anxiety-like behavior in the open field assay of WT or APP/PS1 mice (Fig. S7a).

In conclusion, minocycline is most effective against AD pathology, i. e., microgliosis, A β levels and cognitive decline, when started before the

onset of microgliosis and when provided continuously.

4. Discussion

Here, we analyzed at different levels of study the early phase of AD using the APP/PS1 mouse model with a focus on microglial activation in the hippocampus. We observed the appearance of microgliosis in the hippocampus at the age of 3–4 months, which coincided with impairments of synaptic function and hippocampus-dependent memory retrieval. At this stage, the hippocampus contained high levels of soluble A β_{42} but no A β plaques. Treatment with minocycline to inhibit microgliosis resulted in a rescue of cognitive function and was most effective when started before the onset of microgliosis.

4.1. Hippocampal microgliosis appears before plaque deposition and coincides with cognitive impairments in APP/PS1 mice

Recent advances have led to the increased recognition that the severity of cognitive impairment in AD correlates well with reactive gliosis and synaptic loss (Merluzzi et al., 2018; Scheff et al., 2006; Terry et al., 1991; Westerman et al., 2002). Very recent work provided genetic support for the role of microglia in late-onset AD (Wightman et al., 2021) and reactive microglia show increased clearing of A β plaques and fibrils (Biscaro et al., 2012; El-Shimy et al., 2015; Familian et al., 2006; Fan et al., 2007; Ferretti et al., 2012; Parachikova et al., 2010; Seabrook et al., 2006). Here, we report that microgliosis, while still absent in the hippocampus of APP/PS1 mice at the age of 2 months, becomes manifest at 3 months of age together with the first signs of synaptic and cognitive impairment, which is well before A β plaques develop in the hippocampus. Our findings are in line with previous research that observed hippocampus-dependent memory deficits before the presence of hippocampal A β plaques in APP/PS1 (Hijazi et al., 2019; Végth et al., 2014; Zhu et al., 2017), J20 (Hong et al., 2016) and Tg2576 AD mouse models (Deacon et al., 2008). It should be noted that whereas the impaired performance we observed for pre-plaque stage APP/PS1 mice in the MWM and by contextual fear conditioning (Végth et al., 2014) implies defective hippocampal function, nest building performance is also influenced by stress and motivation and therefore relies next to hippocampal function also on the amygdala and prefrontal cortex (Deacon,

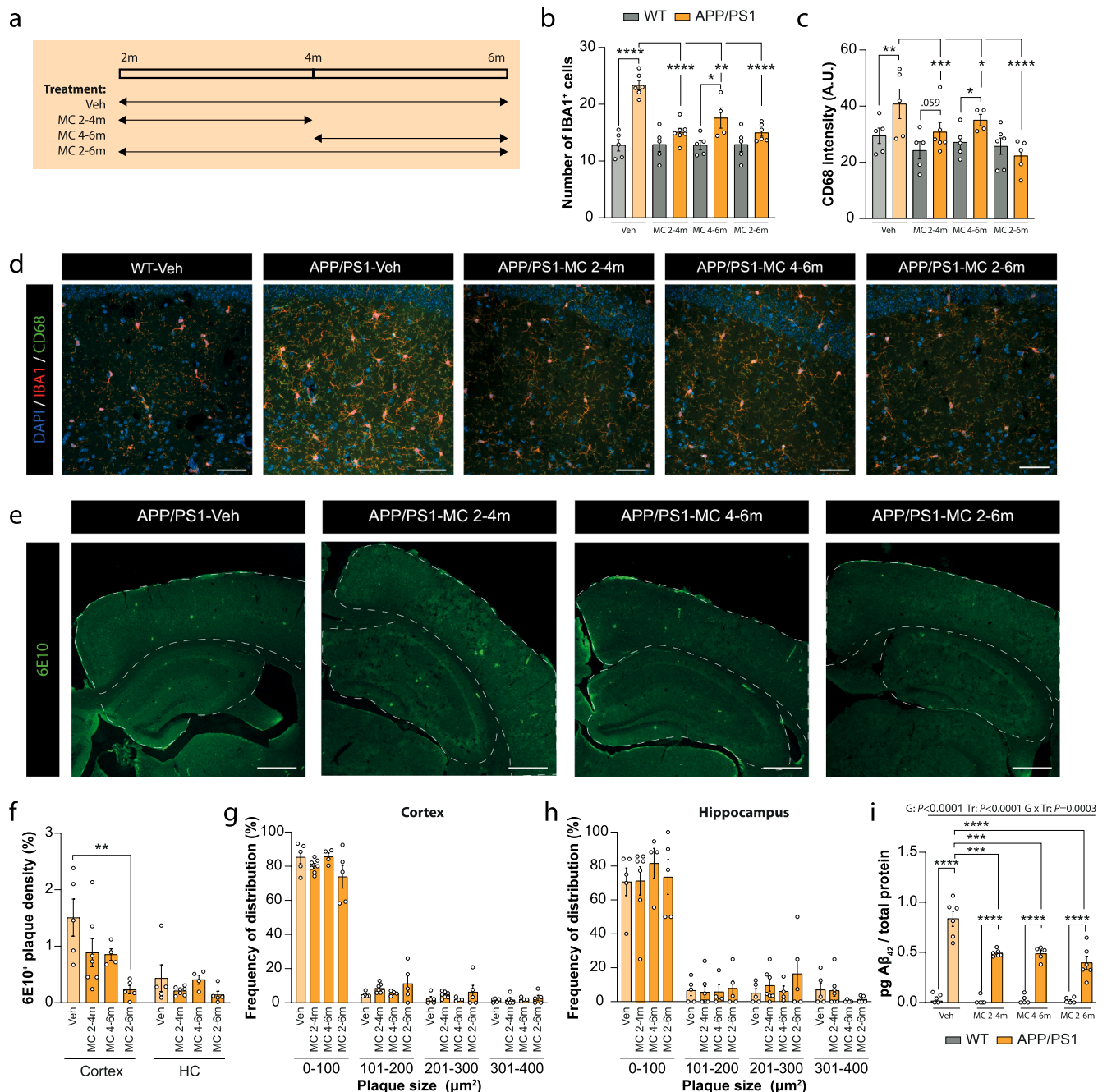


Fig. 8. Reduction of microgliosis by minocycline in APP/PS1 mice is most effective when provided before the onset of microgliosis and upon continuous exposure. a) Schematic overview of experimental workflow. b) Representative images of IBA1 and CD68 staining in hippocampal CA1. Scale bar = 50 μ m c) Quantification of number of IBA1⁺ cells measured in the hippocampal CA1 per field of view (318.20 \times 318.20 μ m). d) Quantification of CD68 staining intensity in arbitrary units (A.U.) measured per IBA1⁺ microglia. e) Representative images of 6E10 antibody staining to identify plaques in cortex and hippocampus of APP/PS1 mice. Scale bar = 500 μ m. f) Quantification of 6E10⁺ plaques density relative to the total cortex or hippocampus region. g) Frequency distribution plot showing plaque size (in μ m²) for cortex. h) Frequency distribution plot showing plaque size (in μ m²) for hippocampus. i) Levels of soluble A β ₄₂ measured by ELISA in hippocampus homogenate. One-way ANOVA (fig. c, f), nested one-way ANOVA (fig. d) or two-way ANOVA (fig. g-i). $n = 4-6$ per group. See table S2 for full statistical details. * $p < 0.05$, ** $p < 0.01$, *** $p < 0.001$, **** $p < 0.0001$. Data are presented as mean \pm SEM.

2006; Deacon et al., 2002; Filali et al., 2009; Gaskill et al., 2013; Neely et al., 2019). Hence, impaired performance in the nest building assays may also relate to the accumulation of A β we observed in the cortex of early-stage APP/PS1 mice (4 months, Fig. 1).

Our observation that early stage APP/PS1 mice are impaired in hippocampal synaptic plasticity is in agreement with previous observations (Smit et al., 2021; Végé et al., 2014; Volianskis et al., 2010), and provides a potential explanation for the behavioral deficits in the MWM, contextual fear conditioning, and nest building tasks. Furthermore, our

data indicate the involvement of synapse loss in this, since a reduction in spine density was observed at apical dendritic trees of pyramidal neurons in the hippocampal CA1. Synapse loss forms an important pathological correlate of AD severity (Terry et al., 1991), and has also been reported for different AD mouse models (Jacobsen et al., 2006; Marchetti & Marie, 2011; Merino-Serrais et al., 2011) including for APP/PS1 mice for which synapse loss was reported in the hippocampus at 7 months of age (Ding et al., 2008; Woo et al., 2015). Here we show that synapse loss is already present in the hippocampus of APP/PS1 mice at

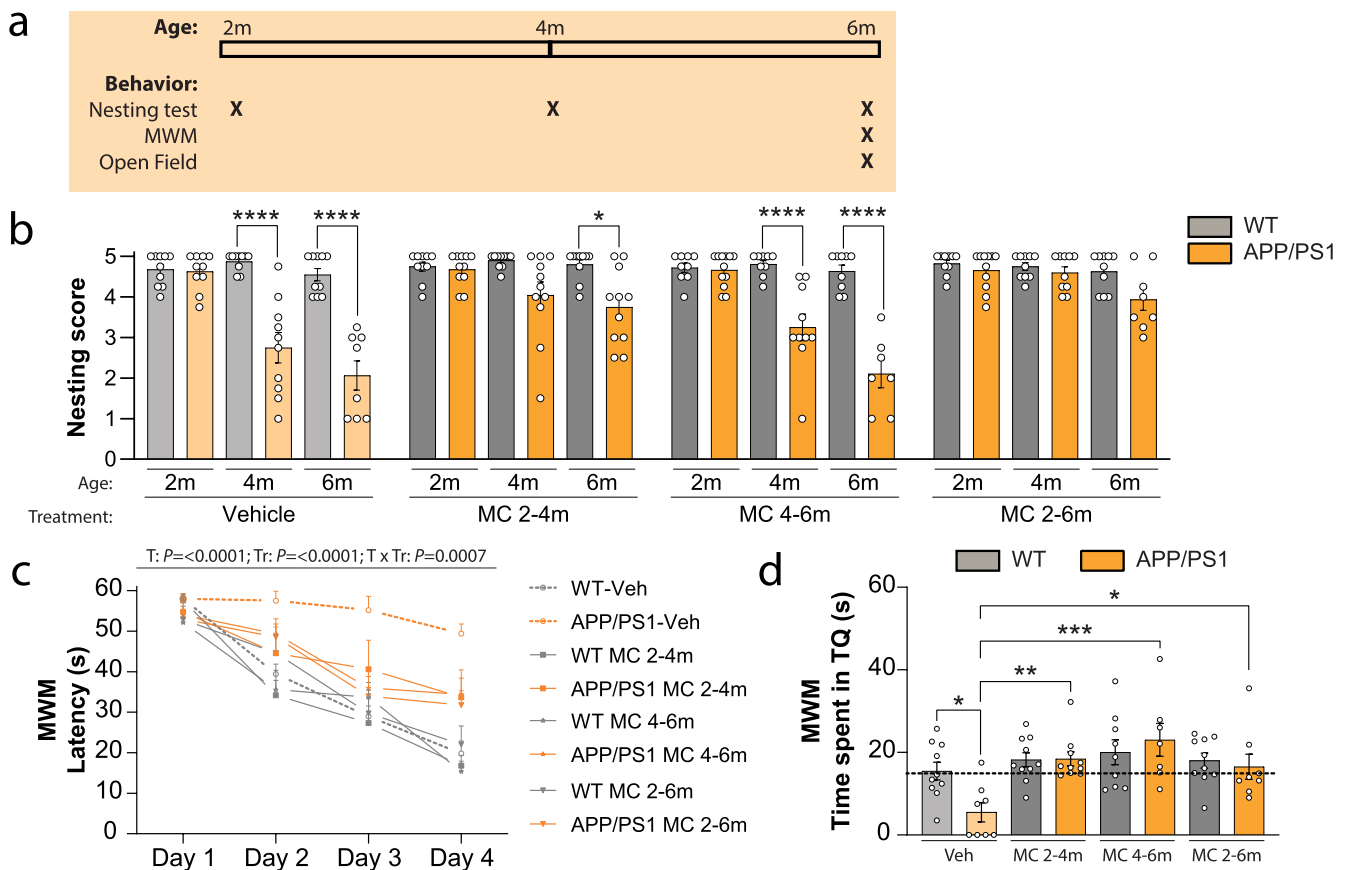


Fig. 9. Cognitive rescue of APP/PS1 mice by minocycline is most effective when provided before the onset of microgliosis and upon continuous exposure. a) Schematic overview of performed cognitive experiments. b) Nesting test scores measured at 2, 4 and 6 months of age. c) MWM training latencies. d) MWM probe test performance. Time spent in target quadrant (TQ) shown only. Dashed line indicates 25 % chance level of exploration. Two-way ANOVA (fig. b), repeated measures ANOVA (fig. c) or one-way ANOVA (fig. d), $n = 7-10$ per group. See table S2 for full statistical details. * $p < 0.05$; ** $p < 0.01$; *** $p < 0.001$; **** $p < 0.0001$. Data are presented as mean \pm SEM.

the pre-plaque stage at 4 months of age. This is suggesting a mechanism in which soluble $A\beta_{42}$, rather than $A\beta$ plaques, triggers microgliosis that subsequently leads to a progressive reduction in the function of synapses and loss of spines. This is supported by the uncoupling of LTP and amyloid deposits by minocycline at 4 months: LTP is rescued by minocycline treatment while amyloid deposits are not.

Taken together, we conclude that microgliosis becomes apparent in the hippocampus of pre-plaque APP/PS1 mice, and coincides with the appearance of memory impairments and synaptic loss. This indicates that microgliosis is one of the initial pathologies in AD, presumably initiated by the progressive increase in $A\beta_{42}$ levels, and potentially implicated in subsequent synaptic and cognitive impairment.

4.2. Prevention of microgliosis by minocycline rescues synaptic plasticity and cognitive behavior with little effect on $A\beta$ levels

To determine a role for microgliosis in early AD pathology, we treated APP/PS1 mice with minocycline and found that a preventive minocycline treatment, started before the onset of microgliosis, is most effective in the inhibition of microgliosis and improvement of cognitive impairment. Minocycline is an established compound for inhibition of microglial reactivation: it inhibits the microgliosis-associated increase in microglia numbers, phagocytic activity and cytokine production (Bischoff et al., 2012; Fan et al., 2007; Ferretti et al., 2012; Parachikova et al., 2010; Seabrook et al., 2006). Accordingly, we found that minocycline treatment of APP/PS1 mice reduced the increase in hippocampal microglial numbers, their increased expression of the phagocytic marker CD68, as well as subtle changes in microglial morphology. In fact, our

morphometrics analysis indicates a shift into an activated state in response to soluble forms of $A\beta$, as activated microglia have an amoeboid-like shape whereas resting state microglia are described as highly ramified (Dubbelaar et al., 2018; Shippy & Ulland, 2020). Microglia morphology after minocycline treatment has been studied by Biscaro et al., (2012) without reporting significant changes, likely due to the lack of a detailed analysis such as the various morphometrics parameters studied here. Together, our observations on microglia number, CD68 levels and morphology demonstrate that minocycline inhibits microglial reactivation in APP/PS1 mice.

While a minocycline treatment of 2 months was effective in improving hippocampal pathology, e.g., microgliosis, synaptic plasticity and contextual memory, of 4 months old APP/PS1 mice, it did not influence soluble $A\beta_{42}$ levels nor plaque deposition in the hippocampus. This suggests a direct causal relation between inhibition of microgliosis and improvement of synaptic plasticity and cognitive behavior downstream apart from the role of amyloidosis. It should be noted that minocycline treatment did cause a delayed reduction of soluble $A\beta_{42}$ levels when APP/PS1 mice were subsequently aged to 6 months, which was independent of the treatment regime. Importantly, the levels of soluble $A\beta_{42}$ in 6 months minocycline treated APP/PS1 mice were still higher than those of 4 months old APP/PS1 mice, which clearly show memory loss, indicating that also the rescue of memory loss in 6 months old APP/PS1 animals is not acting via affecting soluble $A\beta_{42}$ levels. Interestingly, minocycline treatment also reduced $A\beta$ plaque load in 6 months old APP/PS1 mice, however only in the cortex and not in the hippocampus, and most prevalent when mice were treated upon continuous exposure (MC 2–6 m). How inhibition of microgliosis leads to a reduction on $A\beta$

plaque load on the long term is unclear. Minocycline treatment did not change APP levels indicating that the observed delayed reduction in A β is not caused by a direct effect on APP expression. Alternatively, minocycline is an antibiotic that also has anti-inflammatory activity, and some non-steroidal anti-inflammatory drugs have been shown to lower A β ₄₂ production by direct modulation of gamma-secretase activity (Weggen et al., 2003). Whether minocycline indeed inhibits secretase activity leading to reduction of A β ₄₂, without effects on APP expression, is an interesting possibility that remains to be determined. Phagocytosis of A β by microglia is thought to contribute to the removal of A β molecules and plaques (Huang et al., 2021; Lee & Landreth, 2010), and we observed that microgliosis increases the expression of the phagocytosis marker CD68 expression. It is therefore surprising that the inhibition of microgliosis and CD68 expression by minocycline treatment did not lead to increased but decreased A β levels and plaques. Studies on the effect of minocycline on phagocytosis of A β by microglia have reported inconsistent results: whereas minocycline did consistently inhibit the inflammatory activity of microglia, its effect on soluble and insoluble A β levels was either a decrease (Parachikova et al., 2010), no change (Biscaro et al., 2012; Fan et al., 2007; Malm et al., 2008) or even an increase (El-Shimy et al., 2015). Alternatively, the inhibition of microgliosis by minocycline may cause a reduction of soluble A β and plaques via indirect pathways, for instance A β plaques were also found reduced in APP/PS1 mice when the excitation/inhibition balance of the hippocampal neuronal network was restored by targeting of interneurons (Hijazi et al., 2019).

Minocycline treatment also rescued the impaired synaptic plasticity observed at the early stages of A β pathology. Beneficial effects of minocycline on synaptic plasticity have been reported previously, and found associated with the reduced expression of the pro-inflammatory cytokines (Liu et al., 2012), which are known to interfere with synaptic plasticity (Griffin et al., 2006; Rebola et al., 2011; Wang et al., 2005; Wang et al., 2015). Microglia may also inhibit synaptic plasticity by phagocytosis of synapses (Hong et al., 2016). Although we found that minocycline reduced the expression of the phagocytic marker CD68, the outcome of this on the phagocytic activity of microglia towards synapses is unclear. Minocycline inhibits microglial phagocytosis of synapses during development or adult memory processes in healthy mice (Schafer et al., 2012; Wang et al., 2020), however, an effect of minocycline on synaptic pruning in AD mice has not yet been reported, and our analysis on the effect of minocycline on spine density was not conclusive on this point.

In line with the rescue of synaptic plasticity, we observe that minocycline treatment prevented memory impairments in APP/PS1 mice. Other studies using AD mouse models already reported improvements of cognitive behavior by minocycline (Choi et al., 2007; Fan et al., 2007; Parachikova et al., 2010; Seabrook et al., 2006), however, an important difference with our study is that we carefully determined the onset of microgliosis first, to be able to start minocycline treatment before the presence of microgliosis. We are therefore able to make a relation between the prevention of microgliosis and its consequences on synaptic function and cognitive behavior in our AD mouse model.

Taken together, we demonstrated that treatment with minocycline before the onset of microgliosis efficiently halts microgliosis, synaptic dysfunction and cognitive impairment, however not A β ₄₂ levels, at a stage that plaque deposition is not yet observed. This suggests a direct causal relation between microgliosis and impairment of synaptic plasticity and cognitive behavior. When animals progressed into the plaques stage, minocycline was most effective in inhibiting microgliosis, synaptic dysfunction and cognition impairment when treatment was started before the onset of microgliosis. At these stages, minocycline also reduced soluble A β ₄₂ levels and plaque loads, but this did not seem to correlate with the improvements found in hippocampal function.

4.3. Clinical relevance of our minocycline study

Tetracycline antibiotics are widely used to treat bacterial infections, and studies on AD have focused on minocycline because of its lipophilicity, causing a better blood–brain barrier penetration than other tetracyclines (Corbett et al., 2012). A recent clinical study by Howard and colleagues (Howard et al., 2020) on people with mild AD determined cognitive functioning using the Bristol Activities of Daily Living Scale (BADLS) and did not find an improvement by minocycline treatment. The participants in this study were diagnosed with mild cognitive impairment and thus the disease is likely to have progressed into the stage of microgliosis and plaque pathology, which could however not be determined. Although comparison with APP/PS1 mice is a large translational leap, our data on the efficacy of differently timed minocycline treatments of APP/PS1 mice show that minocycline is less effective in the inhibition of microgliosis and rescue of cognitive function when microgliosis is already apparent. This is especially true for the nest building task that has been suggested to have high translational value as nesting behavior might mirror ‘activities of daily living’ (ADL) in humans (Deacon, 2014) and therefore may relate to the BADLS as used in the clinical study by Howard and colleagues. Our observations on APP/PS1 mice that only pre-symptomatic and continuous minocycline treatment was able to successfully rescue impaired nest building, while post-symptomatic treatment was not, indicates that minocycline should be provided before the onset of microgliosis, and furthermore continuously, for the best outcome on microgliosis, plaque depositions and cognitive function.

4.4. Minocycline adverse effects

Short term exposures with tetracyclines are generally well tolerated in older people (Corbett et al., 2012), but a clinical study in AD indicates that exposure for 24 months with 400 mg minocycline is poorly tolerated (Howard et al., 2020). In a pilot experiment, we observed that exposure of mice with 50 mg/kg minocycline via intra peritoneal injection was not tolerated well, as has also been described by Ferreti et al., 2012. We therefore continued to administer 50 mg/kg minocycline orally, which was tolerated well. Besides the inhibition of microgliosis in APP/PS1 mice, and consequent rescue of LTP and memory deficits, we also observed remarkable effects of minocycline on WT animals. Treatment of WT mice with minocycline affected microglia morphology in a way that the ramified microglia (cluster 1 in Fig. 4h, i), present in untreated WT, now became absent as was also observed in untreated APP/PS1 mice. However, minocycline does not affect microglia number, nor CD68 expression in WT, indicating that minocycline does not increase microglia reactivity as seen with microgliosis, and rather may have a direct effect on cell morphology and motility, possibly via its described interactions with membranes (Antonenko et al., 2010) or β -integrin expression (Nutile-McMenemy et al., 2007). According to these findings, microglia morphology is not always reflecting their functional properties, making it important to combine morphometric analysis with other parameters of reactivation, such as cell number and phagocytic activity. Furthermore, it is remarkable that minocycline inhibited LTP in WT animals, without having effects on cognitive behavior in WT animals, while it normalized LTP and cognitive behavior in APP/PS1 mice. The underlying cause of the effect of minocycline on LTP in WT animals is unclear, but may involve potential adverse effects of minocycline on gut microbial composition (Distrutti et al., 2014; Mohle et al., 2016; Schmidtner et al., 2019). Moreover, it should be noted that administration of minocycline to healthy human subjects was reported to inhibit spatial memory encoding likely through disruption of striatal processing, not hippocampal (Berens et al., 2020). Even though minocycline was well tolerated by WT mice, and did not affect their natural cognitive behavior, its use in determining the role of microgliosis, and associated morphology, in synaptic plasticity should be taken with caution.

In summary, our results are the first to give a detailed temporal description of early-stage pathogenesis in the hippocampus of APP/PS1 mice. Soluble A β ₄₂, microgliosis and hippocampal-associated memory deficits all manifest together, before the aggregation of A β into plaques. This enabled us to be the first in starting minocycline treatment right before the onset of microgliosis, a timing that we found was most efficient in the prevention of synaptic and cognitive deficits. Preventive treatment with minocycline rescued microgliosis, synaptic plasticity and cognitive function in the hippocampus of APP/PS1 mice without significant effects on soluble A β ₄₂ and plaques. This indicates that microgliosis acts downstream of amyloidosis and mediates its effects on synaptic plasticity and associated memory function. We are furthermore the first to show that a preventive treatment with minocycline should be provided with continuous exposure to prevent recurring microgliosis and consequently cognitive decline. Despite minocycline being effective in preventing cognitive impairment early in APP/PS1 mice, its use in investigating and treating dementia should be done with caution, as already apparent from human clinical studies, but also because its adverse effects on microglia morphology and LTP in WT animals. Based on our findings we conclude that reactivity of microglia is driving early AD progression in APP/PS1 mice, and our data supports that treatment of AD should be aimed at the prevention of microgliosis.

Funding

This work was supported by a Memorabel-ZonMw grant (733050816, 2017).

Declaration of Competing Interest

The authors declare that they have no known competing financial interests or personal relationships that could have appeared to influence the work reported in this paper.

Data availability

Data will be made available on request.

Acknowledgements

The authors would like to thank Iris Bosch and Kyra Swildens (VU University, Amsterdam, The Netherlands) for acquiring microscopic images and the analysis of IHC parameters, Yvonne Gouwenberg (VU University, Amsterdam) for performing immunoblotting and Hilmar van Weering, Tjalling Nijboer and Maaïke Brummer (University Medical Center Groningen, The Netherlands) for help with microglia morphometric analysis.

Appendix A. Supplementary data

Supplementary data to this article can be found online at <https://doi.org/10.1016/j.bbi.2022.10.009>.

References

- Aarts, E., Maroteaux, G., Loos, M., Koopmans, B., Kovačević, J., Smit, A.B., Verhage, M., Sluis, S.v.d., 2015. The light spot test: measuring anxiety in mice in an automated home-cage environment. *Behav. Brain Res.* 294, 123–130. <https://doi.org/10.1016/j.bbr.2015.06.011>.
- Antonenko, Y.N., Rokitskaya, T.I., Cooper, A.J., Krasnikov, B.F., 2010. Minocycline chelates Ca²⁺, binds to membranes, and depolarizes mitochondria by formation of Ca²⁺-dependent ion channels. *J. Bioenerg. Biomembr.* 42 (2), 151–163. <https://doi.org/10.1007/s10863-010-9271-1>.
- Berens, S.C., Bird, C.M., Harrison, N.A., 2020. Minocycline differentially modulates human spatial memory systems. *Neuropsychopharmacology* 45 (13), 2162–2169. <https://doi.org/10.1038/s41386-020-00811-8>.
- Bessis, A., Bechade, C., Bernard, D., Roumier, A., 2007. Microglial control of neuronal death and synaptic properties. *Glia* 55 (3), 233–238. <https://doi.org/10.1002/glia.20459>.
- Biscaro, B., Lindvall, O., Tesco, G., Ekdahl, C.T., Nitsch, R.M., 2012. Inhibition of microglial activation protects hippocampal neurogenesis and improves cognitive deficits in a transgenic mouse model for Alzheimer's disease. *Neurodegenerative Diseases* 9 (4), 187–198. <https://doi.org/10.1159/000330363>.
- Blum, D., Chtarto, A., Tenenbaum, L., Brothi, J., Levivier, M., 2004. Clinical potential of minocycline for neurodegenerative disorders. *Neurobiol. Disease* 17 (3), 359–366. <https://doi.org/10.1016/j.nbd.2004.07.012>.
- Çetereisi, D., Kramvis, I., Gebuis, T., van der Loo, R.J., Gouwenberg, Y., Mansvelder, H. D., Li, K.W., Smit, A.B., Spijker, S., 2019. Gpr158 deficiency impacts hippocampal CA1 neuronal excitability, dendritic architecture, and affects spatial learning. *Front. Cell. Neurosci.* 13 (465) <https://doi.org/10.3389/fncel.2019.00465>.
- Choi, Y., Kim, H.S., Shin, K.Y., Kim, E.M., Kim, M., Kim, H.S., Park, C.H., Jeong, Y.H., Yoo, J., Lee, J.P., Chang, K.A., Kim, S., Suh, Y.H., 2007. Minocycline attenuates neuronal cell death and improves cognitive impairment in Alzheimer's disease models. *Neuropsychopharmacology* 32 (11), 2393–2404. <https://doi.org/10.1038/sj.npp.1301377>.
- Corbett, A., Pickett, J., Burns, A., Corcoran, J., Dunnett, S.B., Edison, P., Hagan, J.J., Holmes, C., Jones, E., Katona, C., Kearns, I., Kehoe, P., Mudher, A., Passmore, A., Shepherd, N., Walsh, F., Ballard, C., 2012. Drug repositioning for Alzheimer's disease. *Nat. Rev. Drug Discov.* 11 (11), 833–846. <https://doi.org/10.1038/nrd3869>.
- D'Amelio, M., Cavallucci, V., Middei, S., Marchetti, C., Pacioni, S., Ferri, A., Diamantini, A., De Zio, D., Carrara, P., Battistini, L., Moreno, S., Bacci, A., Ammassari-Teule, M., Marie, H., Cecconi, F., 2011. Caspase-3 triggers early synaptic dysfunction in a mouse model of Alzheimer's disease. *Nat. Neurosci.* 14 (1), 69–79. <https://doi.org/10.1038/nn.2709>.
- De Strooper, B., Karran, E., 2016. The cellular phase of Alzheimer's disease. *Cell* 164 (4), 603–615. <https://doi.org/10.1016/j.cell.2015.12.056>.
- Deacon, R.M.J., 2006. Assessing nest building in mice. *Nat. Protoc.* 1 (3), 1117–1119.
- Deacon, R.M.J., 2014. A novel approach to discovering treatments for Alzheimer's Disease. *J. Alzheimer's Disease Parkinsonism* 4 (2). <https://doi.org/10.4172/2161-0460.1000142>.
- Deacon, R.M.J., Croucher, A., Rawlins, J.N.P., 2002. Hippocampal cytotoxic lesion effects on species-typical behaviours in mice. *Behav. Brain Res.* 132 (2), 203–213. [https://doi.org/10.1016/S0166-4328\(01\)00401-6](https://doi.org/10.1016/S0166-4328(01)00401-6).
- Deacon, R.M.J., Cholerton, L.L., Talbot, K., Nair-Roberts, R.G., Sanderson, D.J., Romberg, C., Koros, E., Bornemann, K.D., Rawlins, J.N.P., 2008. Age-dependent and -independent behavioral deficits in Tg2576 mice. *Behav. Brain Res.* 189, 126–138. <https://doi.org/10.1016/j.bbr.2007.12.024>.
- Ding, Y., Qiao, A., Wang, Z., Goodwin, J.S., Lee, E.S., Block, M.L., Allsbrook, M., McDonald, M.P., Fan, G.H., 2008. Retinoic acid attenuates β -amyloid deposition and rescues memory deficits in an Alzheimer's disease transgenic mouse model. *J. Neurosci.* 28 (45) <https://doi.org/10.1523/JNEUROSCI.3153-08.2008>.
- Distrutti, E., O'Reilly, J.-A., McDonald, C., Cipriani, S., Renga, B., Lynch, M.A., Fiorucci, S., Sakakibara, M., 2014. Modulation of intestinal microbiota by the probiotic VSL#3 resets brain gene expression and ameliorates the age-related deficit in LTP. *PLoS ONE* 9 (9), e106503.
- Dubbelaar, M.L., Kracht, L., Eggen, B.J.L., Boddeke, E.W.G.M., 2018. The kaleidoscope of microglial phenotypes. *Front. Immunol.* 9 (1753) <https://doi.org/10.3389/fimmu.2018.01753>.
- El-Shimy, I.A., Heikal, O.A., Hamdi, N., 2015. Minocycline attenuates A β oligomers-induced pro-inflammatory phenotype in primary microglia while enhancing A β fibrils phagocytosis. *Neurosci. Lett.* 609, 36–41. <https://doi.org/10.1016/j.neulet.2015.10.024>.
- Familian, A., Boshuizen, R.S., Eikelenboom, P., Veerhuis, R., 2006. Inhibitory effect of minocycline on amyloid β fibril formation and human microglial activation. *Glia* 53 (3), 233–240. <https://doi.org/10.1002/glia.20268>.
- Fan, R., Xu, F., Previti, M.L., Davis, J., Grande, A.M., Robinson, J.K., Van Nostrand, W.E., 2007. Minocycline reduces microglial activation and improves behavioral deficits in a transgenic model of cerebral microvascular amyloid. *J. Neurosci.* 27 (12), 3057–3063. <https://doi.org/10.1523/JNEUROSCI.4371-06.2007>.
- Ferretti, M.T., Allard, S., Partridge, V., Ducatenzeiler, A., Cuello, A.C., 2012. Minocycline corrects early, pre-plaque neuroinflammation and inhibits BACE-1 in a transgenic model of Alzheimer's disease-like amyloid pathology. *J. Neuroinflammation* 9 (62). <https://doi.org/10.1186/1742-2094-9-62>.
- Filali, M., Lalonde, R., Rivest, S., 2009. Cognitive and non-cognitive behaviors in an APPsw/PS1 bigenic model of Alzheimer's disease. *Genes, Brain and Behavior* 8 (2), 143–148. <https://doi.org/10.1111/j.1601-183X.2008.00453.x>.
- Ganz, A.B., Beker, N., Hulsman, M., Sikkes, S., Netherlands Brain, B., Scheltens, P., Smit, A.B., Rozemuller, A.J.M., Hoozemans, J.J.M., Holstege, H., 2018. Neuropathology and cognitive performance in self-reported cognitively healthy centenarians. *Acta Neuropathol. Commun.* 6 (1), 64. <https://doi.org/10.1186/s40478-018-0558-5>.
- Gaskill, B.N., Karas, A.Z., Garner, J.P., Pritchett-Corning, K.R., 2013. Nest building as an indicator of health and welfare in laboratory mice. *J. Visualized Experiments* 82, e51012.
- Gerrits, E., Brouwer, N., Kooistra, S.M., Woodbury, M.E., Vermeiren, Y., Lambourne, M., Mulder, J., Kummer, M., Moller, T., Biber, K., Dunnen, W., De Deyn, P.P., Eggen, B.J. L., Boddeke, E., 2021. Distinct amyloid-beta and tau-associated microglia profiles in Alzheimer's disease. *Acta Neuropathol.* 141 (5), 681–696. <https://doi.org/10.1007/s00401-021-02263-w>.
- Gomez-Nicola, D., Perry, V.H., 2015. Microglial dynamics and role in the healthy and diseased brain: a paradigm of functional plasticity. *Neuroscientist* 21 (2), 169–184. <https://doi.org/10.1177/1073858414530512>.

- Griffin, R., Nally, R., Nolan, Y., McCartney, Y., Linden, J., Lynch, M.A., 2006. The age-related attenuation in long-term potentiation is associated with microglial activation. *J. Neurochem.* 99 (4), 1263–1272.
- Hammond, T.R., Robinton, D., Stevens, B., 2018. Microglia and the brain: complementary partners in development and disease. *Annu. Rev. Cell Dev. Biol.* 34, 523–544. <https://doi.org/10.1146/annurev-cellbio-100616-060509>.
- Hijazi, S., Heisteck, T. S., Scheltens, P., Neumann, U., Shimshek, D. R., Mansvelder, H. D., Smit, A. B., & van Kesteren, R. E. (2019). Early restoration of parvalbumin interneuron activity prevents memory loss and network hyperexcitability in a mouse model of Alzheimer's disease. *Molecular Psychiatry*, 25, 3380–3398. doi: 10.1038/s41380-019-0483-4.
- Holtman, I.R., Raj, D.D., Miller, J.A., Schaafsma, W., Yin, Z., Brouwer, N., Wes, P.D., Moller, T., Orre, M., Kamphuis, W., Hol, E.M., Boddeke, E.W., Eggen, B.J., 2015. Induction of a common microglia gene expression signature by aging and neurodegenerative conditions: a co-expression meta-analysis. *Acta Neuropathol. Commun.* 3, 31. <https://doi.org/10.1186/s40478-015-0203-5>.
- Hong, S., Beja-Glasser, V.F., Nfonoyim, B.M., Frouin, A., Li, S., Ramakrishnan, S., Merry, K.M., Shi, Q., Rosenthal, A., Barres, B.A., Lemere, C.A., Selkoe, D.J., Stevens, B., 2016. Complement and microglia mediate early synapse loss in Alzheimer mouse models. *Science* 352 (6286), 712–716. <https://doi.org/10.1126/science.aad8373>.
- Howard, R., Zubko, O., Bradley, R., Harper, E., Pank, L., O'Brien, J., Fox, C., Tabet, N., Livingston, G., Benthall, P., McShane, R., Burns, A., Ritchie, C., Reeves, S., Lovestone, S., Ballard, C., Noble, W., Nilforooshan, R., Wilcock, G., Gray, R., 2020. Minocycline at 2 different dosages vs placebo for patients with mild Alzheimer disease: a randomized clinical trial. *JAMA Neurol.* 77 (2), 164–174. <https://doi.org/10.1001/jamaneurol.2019.3762>.
- Huang, Y., Happonen, K.E., Burrola, P.G., O'Connor, C., Hah, N., Huang, L., Nimmerjahn, A., Lemke, G., 2021. Microglia use TAM receptors to detect and engulf amyloid beta plaques. *Nat. Immunol.* 22 (5), 586–594. <https://doi.org/10.1038/s41590-021-00913-5>.
- Huffels, C.F.M., Osborn, L.M., Hulshof, L.A., Kooijman, L., Henning, L., Steinhäuser, C., Hol, E.M., 2022. Amyloid-beta plaques affect astrocyte Kir4.1 protein expression but not function in the dentate gyrus of APP/PS1 mice. *Glia* 70 (4), 748–767. <https://doi.org/10.1002/glia.24137>.
- Jacobsen, J.S., Wu, C.-C., Redwine, J.M., Comery, T.A., Arias, R., Bowlby, M., Martone, R., Morrison, J.H., Pangalos, M.N., Reinhart, P.H., Bloom, F.E., 2006. Early-onset behavioral and synaptic deficits in a mouse model of Alzheimer's disease. *PNAS* 103 (13), 5161–5166.
- Jankowsky, J.L., Slunt, H.H., Gonzales, V., Jenkins, N.A., Copeland, N.G., Borchelt, D.R., 2004. APP processing and amyloid deposition in mice haplo-insufficient for presenilin 1. *Neurobiol. Aging* 25 (7), 885–892. <https://doi.org/10.1016/j.neurobiolaging.2003.09.008>.
- Kamphuis, W., Orre, M., Kooijman, L., Dahmen, M., Hol, E.M., 2012. Differential cell proliferation in the cortex of the APPswePS1dE9 Alzheimer's disease mouse model. *Glia* 60 (4), 615–629. <https://doi.org/10.1002/glia.22295>.
- Kamphuis, W., Kooijman, L., Schettters, S., Orre, M., Hol, E.M., 2016. Transcriptional profiling of CD11c-positive microglia accumulating around amyloid plaques in a mouse model for Alzheimer's disease. *Biochim. Biophys. Acta, Mol. Cell. Biol. Lipids* 1862 (10), 1847–1860. <https://doi.org/10.1016/j.bbalis.2016.07.007>.
- Kettenmann, H., Kirchhoff, F., Verkhratsky, A., 2013. Microglia: new roles for the synaptic stripper. *Neuron* 77 (1), 10–18. <https://doi.org/10.1016/j.neuron.2012.12.023>.
- Ladner, C.L., Yang, J., Turner, R.J., Edwards, R.A., 2004. Visible fluorescent detection of proteins in polyacrylamide gels without staining. *Anal. Biochem.* 326 (1), 13–20. <https://doi.org/10.1016/j.ab.2003.10.047>.
- Lee, C.Y., Landreth, G.E., 2010. The role of microglia in amyloid clearance from the AD brain. *J. Neural Transm.* 117 (8), 949–960. <https://doi.org/10.1007/s00702-010-0433-4>.
- Leyh, J., Paeschke, S., Mages, B., Michalski, D., Nowicki, M., Bechmann, I., Winter, K., 2021. Classification of Microglial Morphological Phenotypes Using Machine Learning. *Front. Cell. Neurosci.* 15, 701673 <https://doi.org/10.3389/fncel.2021.701673>.
- Liu, M. C., Liu, X. Q., Wang, W., Shen, X. F., Che, H. L., Guo, Y. Y., Zhao, M. G., Chen, J. Y., & Luo, W. J. (2012). Involvement of Microglia Activation in the Lead Induced Long-Term Potentiation Impairment. *PLoS ONE*, 7(8). 10.1371/journal.pone.0043924.
- Malm, T.M., Magga, J., Kuh, G.F., Vatanen, T., Koistinaho, M., Koistinaho, J., 2008. Minocycline reduces engraftment and activation of bone marrow-derived cells but sustains their phagocytic activity in a mouse model of Alzheimer's disease. *Glia* 56 (16), 1767–1779. <https://doi.org/10.1002/glia.20726>.
- Marchetti, M., Marie, H., 2011. Hippocampal synaptic plasticity in Alzheimer's disease: What have we learned so far from transgenic models? *Rev. Neurosci.* 22 (4), 373–402. <https://doi.org/10.1515/rns.2011.035>.
- Mattei, D., Ivanov, A., Ferrai, C., Jordan, P., Guneykaya, D., Buonfiglioli, A., Schaafsma, W., Przanowski, P., Deuther-Conrad, W., Brust, P., Hesse, S., Patt, M., Sabri, O., Ross, T.J.L., Eggen, B.J.L., Boddeke, E.W.G.M., Kaminska, B., Beule, D., Pombo, A., Kettenmann, H., Wolf, S.A., 2017. Maternal immune activation results in complex microglial transcriptome signature in the adult offspring that is reversed by minocycline treatment. *Transl. Psychiatry* 7 (5), e1120.
- Meijering, E.H.W., Niessen, W.J., Viergever, M.A., 2001. Quantitative evaluation of convolution-based methods for medical image interpolation. *Med. Image Anal.* 5 (2), 111–126. [https://doi.org/10.1016/s1361-8415\(00\)00040-2](https://doi.org/10.1016/s1361-8415(00)00040-2).
- Merino-Serrais, P., Knafo, S., Alonso-Nanclares, L., Feraud-Espinosa, I., Defelipe, J., 2011. Layer-specific alterations to CA1 dendritic spines in a mouse model of Alzheimer's disease. *Hippocampus* 21 (10), 1037–1044. <https://doi.org/10.1002/hipo.20861>.
- Merluzzi, A.P., Carlsson, C.M., Johnson, S.C., Schindler, S.E., Asthana, S., Blennow, K., Zetterberg, H., Bendlin, B.B., 2018. Neurodegeneration, synaptic dysfunction, and gliosis are phenotypic of Alzheimer dementia. *Neurology* 91 (5), E436–E443. <https://doi.org/10.1212/wnl.0000000000005901>.
- Mohle, L., Mattei, D., Heimesaat, M.M., Bereswill, S., Fischer, A., Alutis, M., French, T., Hambardzumyan, D., Matzinger, P., Dunay, I.R., Wolf, S.A., 2016. Ly6C(hi) monocytes provide a link between antibiotic-induced changes in gut microbiota and adult hippocampal neurogenesis. *Cell Rep.* 15 (9), 1945–1956. <https://doi.org/10.1016/j.celrep.2016.04.074>.
- Neely, C.L.C., Pedemonte, K.A., Boggs, K.N., Flinn, J.M., 2019. Nest building behavior as an early indicator of behavioral deficits in mice. *J. Visualized Experiments* 152, e60139.
- Nutile-McMenemy, N., Elfenbein, A., Deleo, J.A., 2007. Minocycline decreases in vitro microglial motility, beta1-integrin, and Kv1.3 channel expression. *J. Neurochem.* 103 (5), 2035–2046. <https://doi.org/10.1111/j.1471-4159.2007.04889.x>.
- Orre, M., Kamphuis, W., Osborn, L.M., Jansen, A.H.P., Kooijman, L., Bossers, K., Hol, E.M., 2014. Isolation of glia from Alzheimer's mice reveals inflammation and dysfunction. *Neurobiol. Aging* 35 (12), 2746–2760. <https://doi.org/10.1016/j.neurobiolaging.2014.06.004>.
- Paolucelli, R.C., Bolasco, G., Pagani, F., Maggi, L., Scianni, M., Panzanelli, P., Giustetto, M., Ferreira, T.A., Guiducci, E., Dumas, L., Ragozzino, D., Gross, C.T., 2011. Synaptic pruning by microglia is necessary for normal brain development. *Science* 333, 1456–1459. <https://doi.org/10.1126/science.1202529>.
- Parachikova, A., Vasilevko, V., Cribbs, D.H., Laferla, F.M., Green, K.N., 2010. Reductions in amyloid- β -derived neuroinflammation, with minocycline, restore cognition but do not significantly affect tau hyperphosphorylation. *J. Alzheimers Dis.* 21 (2), 527–542. <https://doi.org/10.3233/jad-2010-100204>.
- Perez-Nievas, B.G., Stein, T.D., Tai, H.C., Dols-Icardo, O., Scotton, T.C., Barroeta-Espar, I., Fernandez-Carballo, L., de Munain, E.L., Perez, J., Marquie, M., Serrano-Pozo, A., Frosch, M.P., Lowe, V., Parisi, J.E., Petersen, R.C., Ikonomic, M.D., Lopez, O.L., Klunk, W., Hyman, B.T., Gomez-Isla, T., 2013. Dissecting phenotypic traits linked to human resilience to Alzheimer's pathology. *Brain* 136 (Pt 8), 2510–2526. <https://doi.org/10.1093/brain/awt171>.
- Querfurth, H.W., LaFerla, F.M., 2010. Alzheimer's disease. *N. Engl. J. Med.* 362 (4), 329–344. <https://doi.org/10.1056/NEJMra0909142>.
- Rebola, N., Simões, A.P., Canas, P.M., Tomé, A.R., Andrade, G.M., Barry, C.E., Agostinho, P.M., Lynch, M.A., Cunha, R.A., 2011. Adenosine A_{2A} receptors control neuroinflammation and consequent hippocampal neuronal dysfunction. *J. Neurochem.* 117 (1), 100–111. <https://doi.org/10.1111/j.1471-4159.2011.01718.x>.
- Risher, W.C., Ustunkaya, T., Singh Alvarado, J., Eroglu, C., Dunaevsky, A., 2014. Rapid golgi analysis method for efficient and unbiased classification of dendritic spines. *PLoS ONE* 9 (9), e107591.
- Sasaguri, H., Nilsson, P., Hashimoto, S., Nagata, K., Saito, T., De Strooper, B., Hardy, J., Vassar, R., Winblad, B., Saido, T.C., 2017. APP mouse models for Alzheimer's disease preclinical studies. *EMBO J.* 36 (17), 2473–2487. <https://doi.org/10.15252/emboj.201797397>.
- Schafer, D.P., Lehrman, E.K., Kautzman, A.G., Koyama, R., Mardinly, A.R., Yamasaki, R., Ransohoff, R.M., Greenberg, M.E., Barres, B.A., Stevens, B., 2012. Microglia sculpt postnatal neural circuits in an activity and complement-dependent manner. *Neuron* 74 (4), 691–705. <https://doi.org/10.1016/j.neuron.2012.03.026>.
- Scheff, S.W., Price, D.A., Schmitt, F.A., Mufson, E.J., 2006. Hippocampal synaptic loss in early Alzheimer's disease and mild cognitive impairment. *Neurobiol. Aging* 27 (10), 1372–1384. <https://doi.org/10.1016/j.neurobiolaging.2005.09.012>.
- Schmidtner, A.K., Slattery, D.A., Glasner, J., Hiergeist, A., Grykka, K., Malik, V.A., Hellmann-Regen, J., Heuser, I., Baghai, T.C., Gessner, A., Rupprecht, R., Di Benedetto, B., Neumann, I.D., 2019. Minocycline alters behavior, microglia and the gut microbiome in a trait-anxiety-dependent manner. *Transl. Psychiatry* 9 (1), 223. <https://doi.org/10.1038/s41398-019-0556-9>.
- Seabrook, T.J., Jiang, L., Maier, M., Lemere, C.A., 2006. Minocycline Affects Microglia Activation, A β Deposition, and Behavior in APP-tg Mice. *Glia* 53, 776–782. <https://doi.org/10.1002/glia.20338>.
- Shi, Q., Chowdhury, S., Ma, R., Le, K.X., Hong, S., Caldarone, B.J., Stevens, B., Lemere, C.A., 2017. Complement C3 deficiency protects against neurodegeneration in aged plaque-rich APP/PS1 mice. *Sci. Transl. Med.* 9 (392) <https://doi.org/10.1126/scitranslmed.aaf6295>.
- Shippy, D.C., Ulland, T.K., 2020. Microglial immunometabolism in Alzheimer's disease. *Front. Cell. Neurosci.* 14 (563446) <https://doi.org/10.3389/fncel.2020.563446>.
- Smit, T., Deshayes, N.A.C., Borchelt, D.R., Kamphuis, W., Middeldorp, J., Hol, E.M., 2021. Reactive astrocytes as treatment targets in Alzheimer's disease—Systematic review of studies using the APPswePS1dE9 mouse model. *Glia* 69 (8), 1852–1881. <https://doi.org/10.1002/glia.23981>.
- Terry, R.D., Masliah, E., Salmon, D.P., Butters, N., DeTeresa, R., Hill, R., Hansen, L.A., Katzman, R., 1991. Physical basis of cognitive alterations in Alzheimer's disease: synapse loss is the major correlate of cognitive impairment. *Ann. Neurol.* 30 (4), 572–580. <https://doi.org/10.1002/ana.410300410>.
- Tremblay, M.E., Stevens, B., Sierra, A., Wake, H., Bessis, A., Nimmerjahn, A., 2011. The role of microglia in the healthy brain. *J. Neurosci.* 31 (45), 16064–16069. <https://doi.org/10.1523/JNEUROSCI.4158-11.2011>.
- Van Tijn, P., Dennissen, F.J.A., Gentier, R.J.G., Hobo, B., Hermes, D., Steinbusch, H.W.M., Van Leeuwen, F.W., Fischer, D.F., 2012. Mutant ubiquitin decreases amyloid β plaque formation in a transgenic mouse model of Alzheimer's disease. *Neurochem. Int.* 61 (5), 739–748. <https://doi.org/10.1016/j.neuint.2012.07.007>.

- Végh, M.J., Heldring, C.M., Kamphuis, W., Hijazi, S., Timmerman, A.J., Li, K.W., van Nierop, P., Mansvelder, H.D., Hol, E.M., Smit, A.B., van Kesteren, R.E., 2014. Reducing hippocampal extracellular matrix reverses early memory deficits in a mouse model of Alzheimer's disease. *Acta Neuropathol. Commun.* 2 (76) <https://doi.org/10.1186/s40478-014-0076-z>.
- Volianskis, A., Kostner, R., Mølgaard, M., Hass, S., Jensen, M.S., 2010. Episodic memory deficits are not related to altered glutamatergic synaptic transmission and plasticity in the CA1 hippocampus of the APPswe/PS1 Δ E9-deleted transgenic mice model of β -amyloidosis. *Neurobiol. Aging* 31 (7), 1173–1187. <https://doi.org/10.1016/j.neurobiolaging.2008.08.005>.
- Wang, W.Y., Tan, M.S., Yu, J.T., Tan, L., 2015. Role of pro-inflammatory cytokines released from microglia in Alzheimer's disease. *Ann. Transl. Med.* 3 (10) <https://doi.org/10.3978/j.issn.2305-5839.2015.03.49>.
- Wang, Q., Wu, J., Rowan, M.J., Anwyl, R., 2005. β -Amyloid inhibition of long-term potentiation is mediated via tumor necrosis factor. *Eur. J. Neurosci.* 22 (11), 2827–2832. <https://doi.org/10.1111/j.1460-9568.2005.04457.x>.
- Wang, C., Yue, H., Hu, Z., Shen, Y., Ma, J., Li, J., Wang, X.D., Wang, L., Sun, B., Shi, P., Wang, L., Gu, Y., 2020. Microglia mediate forgetting via complement-dependent synaptic elimination. *Science* 367 (6478), 688–694. <https://doi.org/10.1126/science.aaz2288>.
- Weggen, S., Eriksen, J.L., Sagi, S.A., Pietrzik, C.U., Ozols, V., Fauq, A., Golde, T.E., Koo, E.H., 2003. Evidence that nonsteroidal anti-inflammatory drugs decrease amyloid β 42 production by direct modulation of gamma-secretase activity. *J. Biol. Chem.* 278 (34), 31831–31837. <https://doi.org/10.1074/jbc.M303592200>.
- Westerman, M.A., Cooper-Blacketer, D., Mariash, A., Kotilinek, L., Kawarabayashi, T., Younkin, L.H., Carlson, G.A., Younkin, S.G., Ashe, K.H., 2002. The relationship between β and memory in the Tg2576 mouse model of Alzheimer's disease. *J. Neurosci.* 22 (5), 1858–1867. <https://doi.org/10.1523/jneurosci.22-05-01858.2002>.
- Wightman, D.P., Jansen, I.E., Savage, J.E., Shadrin, A.A., Bahrami, S., Holland, D., Rongve, A., Borte, S., Winsvold, B.S., Drange, O.K., Martinsen, A.E., Skogholt, A.H., Willer, C., Bråthen, G., Bosnes, I., Nielsen, J.B., Fritsche, L.G., Thomas, L.F., Pedersen, L.M., Gabrielsen, M.E., Johnsen, M.B., Meisingset, T.W., Zhou, W., Proitsi, P., Hodges, A., Dobson, R., Velayudhan, L., Heilbron, K., Auton, A., Agee, M., Aslibekyan, S., Babalola, E., Bell, R.K., Bielenberg, J., Bryc, K., Bullis, E., Cameron, B., Coker, D., Partida, G.C., Dhamija, D., Das, S., Elson, S.L., Filshtein, T., Fletez-Brant, K., Fontanillas, P., Freyman, W., Gandhi, P.M., Hicks, B., Hinds, D.A., Huber, K.E., Jewett, E.M., Jiang, Y., Kleinman, A., Kukar, K., Lane, V., Lin, K.-H., Lowe, M., Luff, M.K., McCreight, J.C., McIntyre, M.H., McManus, K.F., Micheletti, S. J., Moreno, M.E., Mountain, J.L., Mozaffari, S.V., Nandakumar, P., Noblin, E.S., O'Connell, J., Petrakovitz, A.A., Poznik, G.D., Schumacher, M., Shastri, A.J., Shelton, J.F., Shi, J., Shringarpure, S., Tian, C., Tran, V., Tung, J.Y., Wang, X., Wang, W., Weldon, C.H., Wilton, P., Sealock, J.M., Davis, L.K., Pedersen, N.L., Reynolds, C.A., Karlsson, I.K., Magnusson, S., Stefansson, H., Thordardottir, S., Jonsson, P.V., Snaedal, J., Zettergren, A., Skoog, I., Kern, S., Waern, M., Zetterberg, H., Blennow, K., Stordal, E., Hveem, K., Zwart, J.-A., Athanasiu, L., Selnes, P., Saltvedt, I., Sando, S.B., Ulstein, I., Djurovic, S., Fladby, T., Aarsland, D., Selbæk, G., Ripke, S., Stefansson, K., Andreassen, O.A., Posthuma, D., 2021. A genome-wide association study with 1,126,563 individuals identifies new risk loci for Alzheimer's disease. *Nat. Genet.* 53 (9), 1276–1282.
- Woo, J.A., Zhao, X., Khan, H., Penn, C., Wang, X., Joly-Amado, A., Weeber, E., Morgan, D., Kang, D.E., 2015. Slingshot-Cofilin activation mediates mitochondrial and synaptic dysfunction via β ligation to β 1-integrin conformers. *Cell Death Differ.* 22 (6), 921–934. <https://doi.org/10.1038/cdd.2015.5>.
- Yong, V.W., Wells, J., Giuliani, F., Casha, S., Power, C., Metz, L.M., 2004. The promise of minocycline in neurology. *Lancet Neurol.* 3 (12), 744–751. [https://doi.org/10.1016/s1474-4422\(04\)00937-8](https://doi.org/10.1016/s1474-4422(04)00937-8).
- Zhang, X., Heng, Y., Kooistra, S.M., van Weering, H.R.J., Brummer, M.L., Gerrits, E., Wesseling, E.M., Brouwer, N., Nijboer, T.W., Dubbelaar, M.L., Boddeke, E.W.G.M., Eggen, B.J.L., 2021. Intrinsic DNA damage repair deficiency results in progressive microglia loss and replacement. *Glia* 69 (3), 729–745. <https://doi.org/10.1002/glia.23925>.
- Zhu, S., Wang, J., Zhang, Y., He, J., Kong, J., Wang, J.F., Li, X.M., 2017. The role of neuroinflammation and amyloid in cognitive impairment in an APP/PS1 transgenic mouse model of Alzheimer's disease. *CNS Neurosci. Ther.* 23 (4), 310–320. <https://doi.org/10.1111/cns.12677>.